Calcium isotope fractionation associated with adsorption and desorption on/from δ-MnO2

Anne-Désirée Schmitt, Sophie Gangloff, Jean-Michel Brazier, Nicolas Nuvoli, Emmanuel Tertre

Calcium isotope fractionation associated with adsorption and desorption on/from δ-MnO_2

Schmitt Anne-Désirée[1*], Gangloff Sophie[1], Brazier Jean-Michel[1,2], Nuvoli Nicolas[1], Tertre Emmanuel[3]

[1] Université de Strasbourg, CNRS, ENGEES, ITES UMR 7063, 5, rue Descartes, 67084 Strasbourg Cédex, France

[2] Present address: Institute of Applied Geosciences, Graz University of Technology, Rechbauerstrasse 12, 8010 Graz, Austria

[3] Université de Poitiers/CNRS, UMR 7285 IC2MP (équipe HydrASA), B8 rue Albert Turpain, 86073 Poitiers, France

* Corresponding author (email: adschmitt@unistra.fr)

Abstract

Small mineral particles present in soils, such as clay minerals and some oxyhydroxides, constitute important nutrient reservoirs. This behavior is due to the negative charges and high specific surface areas of these particles allowing them to adsorb cations such as calcium (Ca), a macronutrient that occupies key physiological and structural functions in plant metabolism. Although the chemical reactivity of clay minerals is rather well-known in the literature, especially toward macronutrients such as Ca, that of oxyhydroxides such as phyllomanganate minerals remains largely unexplored.

To enhance our understanding of the mechanisms at the origin of the storage/release of the different isotopes of Ca in a soil solution, the possible fractionation between ^{40}Ca and ^{44}Ca during adsorption and desorption of Ca on a synthetic phyllomanganate, abiotically precipitated in the laboratory [synthetic analog of vernadite (δ-MnO_2)], was studied. Experiments were performed in batch (closed system), and several parameters (time, pH of the solution, Ca

concentration and nature and concentration of the desorbent) were tested to cover a large range of physicochemical conditions.

This study demonstrated that the light ^{40}Ca isotope is preferentially adsorbed on δ-MnO_2, with $\Delta^{44/40}Ca$ (the apparent fractionation between initial and final conditions) of the adsorbed Ca that can reach 1.19 ± 0.15 ‰"The results showed that this isotopic fractionation occurs at chemical equilibrium in a closed system and that the isotopic fractionation measured in this study during Ca adsorption on phyllomanganate is significantly higher than that reported in the literature during Ca adsorption on other soil constituents such as clay minerals. At pH below 4 Ca occupies only the interlayer/basal sites whereas above this pH it fills first the interlayer/basal sites (~86%) and then edges sites (~14%). By combining the experimental data obtained at different pH values, initial Ca concentrations and interaction times, our results suggest that isotopic signature of the Ca adsorbed on δ-MnO_2 is dependent on the nature of the site involved in the adsorption step (i.e., enriched in ^{40}Ca in the interlayer with $\Delta^{44/40}Ca$ equal to -0.43‰ and enriched in ^{44}Ca when bound to the edges with $\Delta^{44/40}Ca$ equal to +3.5‰). As revealed by surface complexation modeling, such contrasting behavior between the two types of adsorption sites could be due to the bidendate nature of the Ca adsorption occurring on edges and to ion exchange of Ca^{2+} with H^+ in the interlayer sites. Finally, desorption experiments point to total but not instantaneous Ca desorption, probably due to a partial collapse of the interlayer with some ions used to desorb Ca^{2+} (K^+, NH_4^+, hexaamine-cobalt). This suggests that the amount of bioavailable Ca in soils by simple ion-exchange reactions is highly dependent on the nature of the ions which could desorb Ca present in the soil solution.

Keywords

Ca isotopes, adsorption/desorption, δ-MnO_2 (vernadite), surface complexation model, fractionation factor

1. Introduction

Sustainable management of forest ecosystems requires better knowledge of the dynamics of nutrients in forest soils. In contrast to other macronutrients, such as nitrogen (N) or phosphorus (P), studies about the dynamics in soils and the availability to plants of calcium (Ca) are not well developed although itis an essential nutrient with key physiological and structural functions in plant metabolism (Marschner, 1995). Field-based studies performed in nutrient-depleted soils (e.g. acidic substratum and/or subject to acidic rain) point to the essential role of nutrients reservoir within soil in the Ca uptake by vegetation (e.g., soil solutions, adsorbed Ca on organo-mineral soil phases, secondary minerals) (Schmitt et al., 2017). Consequently, it appears essential to precisely identify and characterize these reservoirs to improve our understanding of the dynamics operating in the different soil reservoirs and the Ca bioavailability for trees.

Over the last decade, , studies of the Ca biogeochemical cycle in the critical zone using the different stable Ca isotopes have revealed isotopic fractionations associated with biotic (taken up by roots and translocation within trees, recycling by vegetation) or abiotic (precipitation of secondary minerals, adsorption/desorption) processes (e.g., Cenki-Tok et al., 2009; Cobert et al., 2011; Schmitt et al., 2012; Bagard et al., 2013; Schmitt et al., 2013; 2017; 2018; Gangloff et al., 2014; Schmitt, 2016; Brazier et al., 2019; 2020; Griffith et al., 2020).

A recent study showed that during the adsorption and desorption of Ca on model phyllosilicates commonly found in soils (i.e., kaolinite KGa-2, montmorillonite Swy2 and Tuftane muscovite sorted in size), the light isotope (^{40}Ca) was preferentially adsorbed/desorbed (relative to ^{44}Ca) and that the amplitude of this fractionation for a given mineral was a function of (i) the particle size fraction considered (0.1–1 µm versus 50-200 µm; i.e., influence of the external specific surface area), (ii) the surface charge (induced in particular by the structural charge due to defects in the considered crystal structures), and (iii) the presence of an interlayer space accessible to

cations (Brazier et al., 2019). In particular, these authors have shown that the most significant isotopic fractionation that has been measured (+ 0.24 ‰, apparent fractionation between solid and reactive solution) was obtained with the small size fraction (0.1–1 µm) of muscovite, suggesting that the structural charge was, at least at zero order, the main force driving the isotopic fractionation for a given size fraction of a phyllosilicate mineral.

In addition to clay minerals, other layered minerals as phyllomanganates are ubiquitous in soils. Therefore, question remains to discuss if parameters governing Ca isotopic fractionation during Ca adsorption on phyllomanganates are the same than those previously obtained for phyllosilicates (Brazier et al., 2019). For example, vernadite, $(Na_{0.24}(H_2O)_{0.72}[Mn^{4+}_{0.94}\square_{0.06}]O_2$, Villalobos et al., 2006), which is a nanocrystalline turbostratic disordered phyllomanganate oxide, is also common as nodules and coatings on minerals found in soils, sediments and rocks (e.g., Burns and Burns, 1977; Dorn et al., 1992; Palumbo et al., 2001). Because of substitutions in its structure, hydrated cations such as Ca^{2+} can be located between the layers of this mineral to compensate for the negative layer charge deficit and can also be adsorbed onto the edges of the particles if these sites are negatively charged (e.g., Lanson et al., 2000; 2002; Grangeon et al., 2012; Manceau et al., 2013; Peňa et al., 2015; Simanova et al., 2015; Grangeon et al., 2017). These minerals therefore have a high chemical reactivity in soils and play a major role in solid-solution interactions (Baize, 1997), especially in the biogeochemical cycles of cationic species.

The main objective of this study is to quantify the isotope fractionation during Ca adsorption and desorption on and from a phyllomanganate. To do this, we abiotically precipitated a synthetic analog of vernadite (δ-MnO_2) in laboratory and performed Ca sorption experiments in batch reactors to test the influence of several parameters (time, pH of the solution, Ca concentration and nature and concentration of the desorbent) on the magnitude of Ca isotopic fractionation during adsorption and desorption on/from δ-MnO_2. The obtained data were interpreted by using a surface complexation model (SCM) to improve our understanding of the

mechanisms leading to the Ca storage/release in soils and to better explain the behavior of some of its natural isotopes (i.e., ^{40}Ca and ^{44}Ca).

2. Materials and methods

2.1 Preparation of δ-MnO_2 minerals

The phyllomanganate used in this work was synthesized in the laboratory following the protocol of Villalobos et al. (2003). For this, three solutions were prepared, containing the following:

1) 28 g (i.e., 0.7 mole) of NaOH in 1440 mL of distilled water
2) 40 g (i.e., 0.25 mole) of $KMnO_4$ in 1280 mL of distilled water
3) 75 g (i.e., 0.37 mole) of $MnCl_2.4H_2O$ in 1280 mL of distilled water

The amounts used correspond to the stoichiometric quantities for the synthesis of δ-MnO_2, therefore avoiding adsorption of Mn^{2+} in excess onto the surfaces of the synthesized material,according to the following reaction proposed by Villalobos et al. (2003) and Marafatto et al. (2018):

$$2\ KMnO_4 + 3\ MnCl_2 + 5\ NaOH \rightarrow 5\ MnO_2 + 2\ KCl + 4\ NaCl + 2\ H_2O + OH^- + Na^+ \quad (1)$$

All of the solution 2) was added slowly to the solution 1) in a borosilicate beaker, previously cleaned with distilled water and 10% HCl, under continuous stirring with a magnetic bar at 400 rpm. Following this, the solution 3) was added to the solution 1)-2) mixture dropwise (3 $mL.min^{-1}$). The brown precipitates that formed were then transferred to 50 mL centrifuge tubes and rinsed following five washing cycles with a 1 M NaCl solution and five rinsing cycles with distilled water. These washing and rinsing cycles consisted of replacing the solutions in the tubes with 1 M NaCl or distilled water followed by a stirring of the mixture solid-solution for 1 hour at 40 rpm on an SB3 Stuart™ rotator and a centrifugation at 4700 rpm for 15 min on a

Thermo Jouan multifunction B4I®. After these cycles, the residue was dried for 72 hours in an oven at 60 °C and gently hand ground in an agate mortar. The grounded solid was then sorted granulometrically (size fraction of 0.1–1 µm) to minimize impurities and match some previous studies using other sorbents (i.e., phyllosilicates) (Brazier et al., 2019). For this, 1 g of raw dried powder was mixed with 50 mL of a deflocculant solution (10^{-2} mol.L^{-1} $Na_4P_2O_7$,$10H_2O$) to disperse the particles as much as possible and thus avoid aggregates. After 24 hours of stirring at 40 rpm on an SB3 Stuart™, size separation was performed according to Stokes' law applied to centrifugation steps, allowing the elimination of particles with sizes out the 0.1–1 µm range (see Reinholdt et al., 2013). These centrifugations were carried out on a Thermo Scientific Heraus Megafuge 40R™ centrifuge and a Beckman Coulter Avanti J-30I™ ultracentrifuge instrument. After the size sorting, the 0.1–1 µm solid was rinsed several times with distilled water by successive centrifugation, supernatant removal, and mixing with new distilled water to remove the desorbent before its drying in an oven at 60°C.

The 0.1-1 µm size fraction powder was then conditioned in mono-ionic form (using Na^+ in our case) to facilitate the interpretation of Ca adsorption. For Na saturation, 0.25 g of powder was mixed with 50 mL of a 1 M NaCl solution (99.99%) (at distilled water pH = 5.6) for nine days. Every three days, the supernatant was replaced with a new NaCl solution (three cycles) to remove the desorbed elements, with the second solution being at pH = 3 (acidified with HCl) to ensure decarbonation of the sample. The samples were then dialyzed with distilled water for five days in dialysis bags (porosity 6-8 kDa) from Spectrum Laboratories Inc™ by filling them with 200 mL of solution (NaCl + δ-MnO_2) and let them equilibrate in 1.5 L of distilled water. This distilled water was renewed every 24 hours until its conductivity is sufficiently low (~ 30 µS.cm^{-1}) and no longer changed, indicating that the dialysis/rinsing was finished. The 0.1–1 µm size fraction powder was then dried in an oven at 60 °C for five days, finely and gently crushed using an agate mortar and stored until it was used (see Brazier et al., 2019).

149 ### 2.2 *Characterization of δ-MnO_2*

150 The synthesized and conditioned final mineral was characterized by performing four types of
151 analyses: (1) A powder X-ray diffraction (XRD) analysis using a Bruker AXS D5000
152 diffractometer at the ITES (Strasbourg, France) was carried out in θ/θ mode by scanning
153 between 3° and 65° with steps of 0.04° every 10 sec. Acquisition was obtained using an X-ray
154 tube equipped with a copper (Cu) anticathode operating at 40 kV and 30 mA. (2) The cation
155 exchange capacity (CEC) was measured at ITES (Strasbourg, France) using the hexaamine
156 cobalt-chloride method described by Ciesielski et al. (1997). Succintly, 100 mg of powder was
157 mixed with 45 ml of 10^{-2} mol. L^{-1} hexaamine cobalt-chloride solution for two hours at 40 rpm
158 on an SB3 Stuart™ rotator at room temperature. The suspensions were then filtered at 0.22 µm
159 using regenerated cellulose filters and elementarily analyzed. (3) The external specific surface
160 area was measured on a Micrometrics Tristar™ at IC2MP (Poitiers, France) according to the
161 Brunauer–Emmett–Teller (BET) method (Brunauer et al., 1938) using the N_2 adsorption
162 isotherm. (4) The chemical composition of the solid δ-MnO_2 was determined by wet chemistry
163 analysis. For this, 50 mg of initial δ-MnO_2 (after Na saturation and before Ca-exchange) and
164 aliquots of final δ-MnO_2 (after Ca adsorption) were digested in Savillex™ beakers with 5 N
165 HCl on a hot plate at 100 °C and then evaporated to dryness. The residues were then converted
166 to HNO_3, evaporated to dryness, and then dissolved in 0.25 M HNO_3 for analysis.

167

168 ### *2.3 Ca-for-Na^+ cation-exchange experiments and Ca desorption procedure*

169 All adsorption and desorption experiments were performed in well-mixed closed reactors
170 ("batch" system) allowing the homogeneity of the medium and by considering the decrease in
171 the Ca concentration of the starting solution due to adsorption. The aqueous concentration of
172 Ca in the initial solution was adjusted to be limiting (i.e., more than 75% of the initial Ca

quantity is adsorbed at steady state) but to still have enough Ca remaining in the reactive solution for isotopic fractionation quantification.

Adsorption experiments were performed with an initial solution prepared using hydrated $Ca(NO_3)_2$ salt (Alfa Aesar 99.99% purity) at room temperature (20 °C) and by considering a 2.5 $g.L^{-1}$ solid/solution ratio. The ionic strength was comprised between 0.009 (at pH 10) and 0.019 $mol.L^{-1}$ (at pH 2) and fixed solely by $Ca(NO_3)_2$, and the reagent used to adjust the pH of the initial solutions between 2 and 10 (i.e., 5.10^{-2} $mol.L^{-1}$ HNO_3 or 5.10^{-2} $mol.L^{-1}$ NaOH). Each experiment consisted of mixing 50 mg of dried δ-MnO_2 (0.1-1 µm Na^+-size fraction) with 20 mL of initial Ca solution and corresponded to a single measurement point. Each mixture was stirred at 40 rpm on an SB3 Stuart™ rotator for a given duration and centrifuged for 5 min at 4000 rpm in a Thermo Jouan multifunction B4-I™ centrifuge. This procedure was used for the following experiments):

1. Adsorption kinetics made of eight measurement points at different time (i.e., 5 min, 10 min, 15 min, 35 min, 65 min, 125 min, ~ 24 h and ~ 48 h; including the 5 min of centrifugation) at pH 7 with initial aqueous Ca concentrations fixed at 2.25 mmol. L^{-1} (i.e., 0.10 mmol/mmol Mn).
2. Adsorption experiments performed at different initial pH values ranging from 2 to 10 (range chosen to match different pH soil environments) with initial Ca concentrations fixed at 2.86 mmol. L^{-1} (i.e., 0.124 mmol/mmol Mn) and an adsorption time reaction of 125 min.
3. Adsorption isotherms performed at different initial aqueous Ca concentration varying from 2.20 to 9.81 mmol. L^{-1} (i.e., 0.098 to 0.436 mmol/mmol Mn) at pH 7 and with an adsorption time of 125 min. This initial aqueous Ca concentrations range was chosen to cover a range from limiting to infinite Ca aqueous reservoir considering the solid/solution ratio used (see discussion).

198 (note that throughout the manuscript, mmol/mmol Mn refers to mmol Ca_{aq}/mmol Mn in the
199 solid or mmol $Ca_{adsorbed}$/mmol Mn in the solid depending on the experimental conditions
200 (adsorption or desorption). After each experiment, the supernatant was removed using a 20-mL
201 syringe and filtered at 0.22 µm using cellulose acetate membrane filters and stored prior to
202 analyses.
203 Additionally, some solid residues recovered after adsorption experiments performed at pH 7
204 using an initial aqueous Ca concentration of 2.86 mmol. L^{-1} were used for Ca desorption
205 experiments. These residues (i.e., slurry remaining after supernatant removal) were weighed to
206 quantify the residual liquid mass, and were then stirred during 2 hours, at room temperature (20
207 °C), with 20 mL of different desorbents: hexamine cobalt-chloride - [$(Co(NH_3)_6Cl_3$] (2.10^{-2}, 10^{-2}
208 and 10^{-1} mol.L^{-1}), ammonium acetate (CH_3COONH_4) (10^{-1} and 1 M) and potassium nitrate
209 (KNO_3) (10^{-2}, 10^{-1} and 1 mol. L^{-1}) (hereafter abbreviated Cohex, NH_4^+ and K^+, respectively).
210 The mixtures were then centrifuged at 4000 rpm for 5 min, the supernatant was taken up and
211 filtered (following the same procedure presented above), and replaced by 20 mL of fresh
212 desorbents that were let to react for 48 h with the residues. This procedure was repeated two
213 additional times with 72 h and 120 h of interaction between fresh desorbents and residues.
214 These leaches will be referred to as "sequential leaches" later in the paper. In parallel, 20 mL
215 of Cohex was added to the slurry for 72 h of interaction (referred to as "cumulative leaching"
216 hereafter).

217 *2.4 Analytical procedures*

218 The evolution of pH with time was measured on an aliquot of each filtered sample using a
219 Metrohm 905 Titrando^{TM} titrator calibrated at 25 °C. Elemental and isotopic analyses were
220 performed at the Cortecs-Pacite platform of the University of Strasbourg at ITES (Strasbourg,
221 France).

222 Aqueous Ca, Na, P and Mn concentrations were measured with an ICP–AES iCAP 6000 Series
223 (ThermoFisher Scientific^{TM}), with detection limits, respectively equal to 0.08, 0.1, 0.1 and 0.01
224 µmol.L^{-1} The repeatability was equal to 5% of the concentration of the sample. The accuracy
225 was assessed by repeated measurements of reference materials (SLRS5, Perade-20, Rain 97,
226 Big-Moose 02, Super 05) during each sequence.

227 For the $\delta^{44/40}$Ca analyses, 0.14 µmol of Ca from each analyzed solution supernatant and
228 digestion product was mixed with 0.01 µmol of Ca from a ^{42}Ca-^{43}Ca double spike (^{42}Ca/^{43}Ca
229 spike ratio of ~5), and this mixture was dried at 70 °C on a hot plate. The mixtures were then
230 dissolved in 2 mol.L^{-1} HNO_3, and chemical separations were performed on a DGA resin normal
231 (TODGA, Triskem^{TM}) according to the procedure of Brazier et al. (2019). Eluted Ca was dried
232 a first time at 70 °C and converted to nitric form with 7 M HNO_3 before a second phase of
233 drying at 70 °C on a hot plate. The total Ca blank for the chemical separation procedure
234 represents less than 1.25 nmol. This represents an average contribution of 0.009% to the Ca
235 present in the sample and will be considered negligible in the rest of this work.

236 The dried residues of the chemical separation were dissolved in 1 to 3 µL of 1 mol.L^{-1} HNO_3
237 and deposited on single tantalum filaments (99.995% purity) previously outgassed and oxidized
238 (under primary vacuum) for the $\delta^{44/40}$Ca measurements. All Ca isotope measurements were
239 performed on a TIMS (ThermoFischer Scientific Triton^{TM}) in static mode (see details in Schmitt
240 et al., 2013 and Brazier et al., 2019). To avoid $\delta^{44/40}Ca_{SRM915a}$ intersession drifts, the ^{42}Ca-^{43}Ca
241 double spike was calibrated at each measurement session by measuring three mixtures
242 composed of NIST SRM 915a standard solution and ^{42}Ca-^{43}Ca double spike following the
243 protocol proposed by Lehn et al. (2013).

244 The measured values were expressed as $\delta^{44/40}$Ca per mil relative to the NIST SRM915a standard
245 (Hippler et al., 2003; Eisenhauer et al., 2004):

$$\partial^{44/40}Ca_{SRM915a}\ (‰) = \left(\frac{\left(\frac{^{44}Ca}{^{40}Ca}\right)_{Sample}}{\left(\frac{^{44}Ca}{^{40}Ca}\right)_{SRM915a}} - 1 \right) \times 1000 \quad (2)$$

To directly assess the apparent isotopic fractionation, our results will be expressed as a difference ($\Delta^{44/40}Ca_i$) between the measured Ca isotopic composition in the final aqueous or solid phase ($\delta^{44/40}Ca_i$) and that of the initial solution ($\delta^{44/40}Ca_{ini}$):

$$\Delta^{44/40}Ca_i\ (‰) = \delta^{44/40}Ca_i - \delta^{44/40}Ca_{ini} \quad (3)$$

where i represents the liquid after adsorption (LAA), the solid after adsorption (SAA) or the liquid after desorption (LAD).

The associated propagated uncertainty (Δ_{error}, in ‰) can be expressed as

$$\Delta_{error\left(\Delta^{44/40}Ca_i\right)} = \sqrt{\left(\Delta_{\delta^{44/40}Ca_i}\right)^2 + \left(\Delta_{\delta^{44/40}Ca_{ini}}\right)^2} \quad (4)$$

The average internal repeatability obtained during the course of the study was 0.07 ‰ based on repeated measurements of NIST SRM 915a (2 SD, N=63). Repeated measurements of the initial Ca solution yielded a value equal to 0.85 ± 0.04 ‰ (2SE, N= 6). The external uncertainty calculated from external long-term sample replicates was equal to 0.11 ‰ (2SD, N=22) for $\delta^{44/40}Ca$ values. Using these values and according to Equation (4), the propagated error associated with $\Delta^{44/40}Ca$ is equal to 0.15 ‰. The accuracy of our measurements was explored through the measurements of an in-house Atlantic seawater standard (1.90‰ ± 0.11, 2SD, N=22) during the same period of time, which showed consistent values with those reported by Hippler et al. (2003) and Heuser et al. (2016 and references therein).

3. Modeling of adsorption experimental data

δ-MnO_2 minerals have a layered structure with cations adsorbed in interlayer, allowing to compensate the negative charge due to cation vacancies in the layer, and possible cations adsorbed onto edge sites (van Genuchten and Peña, 2016; Marafatto et al., 2018). Thus, to model the experimental data of Ca^{2+} adsorption on δ-MnO_2, two types of adsorption sites on two different surfaces are considered. The first type of site corresponds to cation exchange sites located in the interlayer/basal surface compensating the negative permanent charges due to the vacancies in the structure (i.e., called $>X^-$ hereafter) and formed during the synthesis of δ-MnO_2 (see below). On/in these sites, the Ca present in solution adsorbs on δ-MnO_2 by an exchange with the compensating cations (Na^+ and/or H^+) electrostatically bounded to the basal/interlayer surfaces (above the vacancies). This cationic exchange can be described by a selectivity coefficient $K_{sel.}$ (Gaines and Thomas, 1953; Bradbury and Baeyens, 2009; Tertre et al., 2011). The reactions of cation exchange can be expressed by the following equations:

$$2{>}X\text{-}Na + Ca^{2+} \leftrightarrow {>}X_2\text{-}Ca + 2Na^+ \quad (5) \qquad K_{sel.(2Na+/Ca2+)}$$

$$2{>}X\text{-}H + Ca^{2+} \leftrightarrow {>}X_2\text{-}Ca + 2H^+ \quad (6) \qquad K_{sel.(2H+/Ca2+)}$$

The second type of sites corresponds to the surface edge sites of the sheets with variable charge depending on the pH (i.e., called >SOH hereafter). Experimental data were modeled by using a geometrical diffuse layer model (DLM). It was used due to its simplicity (i.e., only K_{edge} as adjustable parameter; no capacitance values to fix; see Table 1). Coupling to protonation/deprotonation of the >SOH sites, the reactions of Ca^{2+} adsorption on these sites can be expressed by the following equations:

$$>SOH + H^+ \leftrightarrow >SOH_2^+ \quad (7) \qquad K_{edge(SOH/SOH2+)}$$

$$>SOH \leftrightarrow >SO^- + H^+ \quad (8) \qquad K_{edge(SOH/SO-)}$$

$$2\ >SOH + Ca^{2+} \leftrightarrow >Ca(SOH)_2 + 2H^+ \quad (9) \qquad K_{edge(2SOH/Ca(SOH)2)}$$

290 The Visual Minteq program (Version 3.1; Gustafsson, 2013) together with the PEST
291 optimization option (**P**arameter **EST**imation; see also http://www.pesthomepage.org) was used
292 to model the experimental data of Ca^{2+} adsorption on δ-MnO_2 considering the two types of
293 adsorption sites mentioned above. The adsorption model was applied to the initial Ca solutions
294 in contact with δ-MnO_2 (see section 4), using the aqueous species constants from the default
295 thermodynamic database associated with Visual Minteq 3.1., and the sites densities (for $>X^-$
296 and >SOH) deduced from experimental data measured in this study.

297

298 **4. Results**

299 4.1 Mineral characterization

300 The acid digestion experiment allowed us to determine the molar ratios Ca/Mn and Na/Mn of
301 the δ-MnO_2 mineral (0.001 and 0.29, respectively). Based on the generic formula for δ-MnO_2
302 minerals ($Na_y(Mn_x\square_a)O_2,H_2O$), and the fact that Na/Mn = y/x+a = 1, and y=4a (Villalobos et
303 al., 2003), the following structural formula can be proposed for the solid:
304 $Na_{0.27}(Mn_{0.93}\square_{0.07})O_2,H_2O$ (M=107.73 $g.mol^{-1}$) in accordance with the literature (Post and
305 Veblen, 1990; Drits et al., 1997; Luo et al., 2000; Villalobos et al., 2003). The solid
306 characterized by this structural formula will be represented by the term "δ-MnO_2" throughout
307 the manuscript. Consequently, the minimum percentage of structural vacancies is equal to 7%.
308 By considering this structural formula, the average Mn oxidation number is equal to 3.93, which
309 is close to that reported by previous authors (between 3.49 and 4.02) (Villalobos et al., 2003;
310 Zhao et al., 2009; Grangeon et al. 2012). Furthermore, the Na^+/Mn_{total} ratio equal to 0.29 in our
311 case is representative of the negative structural charge of the solid (Villalobos et al., 2003) and
312 gives an indication of the layer charge per cell value.
313 The CEC and BET N_2 specific surface area values measured in this work on the 0.1-1 µm size
314 fraction of the Na^+- δ-MnO_2 synthesized grains are presented in Table 2. The CEC is rather high

315 (215 meq/100 g) compared to those of the previous phyllosilicate minerals used for similar
316 experiments (see Table 2). The percentage of the CEC represented by Na cations in the initial
317 solids was calculated (see Table 2) and was higher than 99%, indicating that Na-homoionic
318 conditioning was effective. The BET specific surface area measured (i.e., 27.6 m^2/g) is in the
319 range of the values that can be found in the literature for MnO_2 solids (from 15 to 290 m^2/g)
320 (e.g., ,–Murray, 1975; Balistrieri and Murray, 1982; Catts and Langmuir, 1986; Burdige et al.,
321 1992; Gotfredsen and Stone, 1994; Nelson et al., 1999; Villalobos et al., 2003; Tonkin et al.,
322 2004; Marafatto et al., 2018) . The value obtained is coherent with those obtained for other
323 materials characterized by the same particle size (see Table 2). The experimental XRD pattern
324 confirmed that δ-MnO_2 is poorly crystallized (see S1 in Appendix A).
325
326 4.2 Calculation of Ca and Na concentrations and mass balance
327 The Ca adsorption and desorption experimental results from the filtered supernatant obtained
328 at the end of the adsorption and desorption steps are presented in Tables 3 and 4. The amount
329 of adsorbed Ca (and desorbed Na) is calculated as the difference between (i) the initial amount
330 of Ca (or Na) in the liquid ($Ca_{ini,}$ = 0.124 mmol/mmol Mn; Na_{ini} = 0.002 mmol/mmol Mn) and
331 (ii) the amount of Ca (or Na) in the supernatant after adsorption (Ca_{LAA}) (or desorption, Na_{LAA})
332 experiments.
333 It has to be noted that the filtration process is never total at the end of the adsorption step
334 procedure, and thus some aqueous Ca remaining in the pores of the slurry after Ca adsorption
335 have to be considered in the calculation of the amount of desorbed Ca (and associated isotopic
336 ratio). These values (i.e., Ca_{LAD_corr}, $\delta^{44/40}Ca_{LAD\_corr}$) are calculated as the difference between
337 the quantity of Ca measured in the supernatant after desorption (Ca_{LAD}, $\delta^{44/40}Ca_{LAD}$) and the
338 sum of Ca remaining in the slurry and present in the desorbent itself (see Brazier et al., 2019
339 for detailed calculations). Applied corrections were not significant in either elemental

concentration (~1% in average) or isotopic measurements (1.5% of the Δ-value in average), and they will no longer be considered in this work.

The dissolution of δ-MnO_2 during the adsorption/desorption experiments can also be neglected. Indeed, no aqueous Mn was detected in the analyzed supernatants (<0.01 µmol. L^{-1}), and the total amount of Ca from dissolution of the solid (0.01 µmol.mg^{-1}) was less than 1% of the Ca coming from the initial solution used for adsorption experiments. Similarly, no P (< 0.1 µmol.L^{-1}) was detected, so that there could be no pyrophosphate adsorption onto MnOx particles nor interferences to subsequent Ca^{2+} adsorption. Finally, for the samples for which the apparent isotopic composition of Ca in both the residual liquid (LAA) and in the solid (SAA) after adsorption were analyzed, we ensured that the mass balance was equilibrated using the equation (see section 4.1):

$$\Delta^{44/40}Ca_{IS} = f \times \Delta^{44/40}Ca_{LAA} + (1-f) \times \Delta^{44/40}Ca_{SAA} \quad (10)$$

with *IS* the initial solution, and *f* is the proportion of Ca remaining in the aqueous phase after the adsorption step.

4.3 Kinetics of Ca adsorption and desorption

After 20 min of adsorption, the amount of Ca remaining in the aqueous phase stabilizes to approximately 1.5 ± 0.9% of the initial Ca, which corresponds to approximately 98.5 ± 0.9% (2SE, N=7) of Ca adsorbed (Table 3; Fig. 1a). In contrast, Ca desorption by Cohex is not complete since beyond 30 min of reaction this amount stabilizes to 72.1 ± 1.4% (2SE, N=6) of adsorbed Ca (Table 4; Fig. 1a).

Isotopically, the first interaction times experience high $\Delta^{44/40}$Ca values of the solution, followed by a decrease (after 15 and 10 min for adsorption and desorption, respectively) and again an increase, whether for adsorption or desorption steps. After 20 (or 15) min of adsorption (desorption), the isotope composition in Ca of the solution stabilizes to approximately $\Delta^{44/40}$Ca = 1.26 ± 0.09 ‰ (2SE, N=5) (0.49 ± 0.07 ‰, 2SE, N=5) (Fig. 1b). Note that the Ca isotope

365 composition of the supernatant after desorption is enriched in the light ^{40}Ca isotope of 0.77 ‰
366 relative to the supernatant after adsorption, pointing to partial desorption.
367 Furthermore, the amount of Ca that is desorbed is linked to the nature of the desorbent used, its
368 concentration and the interaction time with the solid (Fig. 2a). The higher the concentration of
369 the desorbent, and the higher the number of successive sequential desorption, the greater the
370 quantity of Ca extracted (Fig. 2a). The maximum quantity of Ca (99.5%) is extracted with 0.1
371 M Cohex and with four successive desorption cycles (2 h + 48 h + 72 h + 120 h) (Fig. 2a). After
372 2 hours of interaction, the apparent isotopic fractionation compositions of the desorbed Ca are
373 variable (from 0.12 ‰ for 0.1 M Cohex to 0.90 ‰ for 0.01 M) (Fig. 2b). For 0.1 M Cohex, the
374 first fractions are enriched in the heavy ^{44}Ca isotope (0.12 ‰ for the first 56.6%), while the
375 more we extract Ca, the more we enrich the aqueous phase in the light ^{40}Ca isotope (-1.17 ‰
376 for the last 8.3%) (Table 4; Fig. 2b). The weighted average $\Delta^{44/40}Ca$ value of the different 0.1
377 M Cohex extractions is -0.12 ± 0.24 ‰, which is equal, within propagated error, to the value of
378 the initial solution (i.e. $\Delta^{44/40}Ca$ =0) used for the experiments, confirming that mass balance is
379 effective.
380
381 4.4 Results of pH and initial Ca concentration
382 4.4.1 pH effect (at Ca equal to 0.124 mmol/mmol Mn and 125-min interaction time)
383 For this experiment, the elemental and isotopic analysis results of the liquid and solid fractions
384 after Ca adsorption are presented in Table 5 and in Fig. 3a and b. For Ca solutions with an initial
385 pH between 2 and 4, the concentrations of adsorbed Ca vary between 0.042 mmol/mmol Mn
386 and 0.118 mmol/mmol Mn. At the same time, an increase in final pH from 2.3 to 5.6 is observed,
387 coinciding with a decrease in H_3O^+ in solution, as well as a variation in desorbed Na
388 concentration from 0.244 mmol/mmol Mn (at pH=2) to 0.202 mmol/mmol Mn (at pH=4). Over
389 this pH range, there is thus an adsorption of H_3O^+ and Ca^{2+} with a desorption of Na^+. For Ca

390 solutions with an initial pH between 6 and 10, the adsorbed Ca concentrations are relatively
391 stable at 0.122 mmol/mmol Mn. At the same time, the final pH decreased with a stabilization
392 of approximately 6.1.
393 In parallel, the isotopic compositions in $\Delta^{44/40}$Ca of the aqueous phase, at the end of the Ca
394 adsorption step, increase from pH 2 to pH 4 from 0.25 to 1.15 ‰ and stabilize above pH 4 at
395 1.23 ± 0.06 (2SE, N=2). Concomitantly, the isotopic compositions of solids vary from -0.43 ‰
396 at pH 2 to -0.06 ‰ at pH 4 to finally attain 0.12 ‰ at pH 10 (Table 5 and Fig. 3b).
397
398 4.4.2 Ca concentration effect (at pH=7 and 125-min interaction time)
399 The results of elemental and isotopic analyses of the supernatant liquid after adsorption and of
400 the solid after the Ca-adsorption step are presented in Table 6 and Figs. 3c and d. At pH 7, when
401 the initial Ca concentration increases from 0.098 mmol/mmol Mn to 0.436 mmol/mmol Mn,
402 the adsorbed Ca concentrations vary between 0.097 mmol/mmol Mn and 0.138 mmol/mmol
403 Mn. During this variation, we also noticed a decrease in pH, initially at 7, from 6.36 to 4.48 and
404 an increase in desorbed Na^+ from 0.184 to 0.229 mmol/mmol Mn (Table 6), suggesting
405 desorption of H^+ and Na^+ during Ca^{2+} adsorption. Such a decrease in pH was also observed by
406 van Genuchten et Peña (2016) during the sorption of cations to δ-MnO_2. The adsorbed Ca
407 concentrations stabilize to approximately 0.129 ± 0.006 (2SE, N=6) mmol/mmol Mn from the
408 initial Ca concentration of 0.127 mmol/mmol Mn, and those of desorbed Na stabilize to
409 approximately 0.226 ± 0.004 (2SE, N=6) (Table 6; Fig. 3c). Isotopically, as the initial Ca
410 concentration increases, $\Delta^{44/40}Ca_{LAA}$ decreases from 1.19 ± 0.01 (2SE, N=2) to stabilize at 0.34
411 ± 0.06 (2SE, N=2) for the largest amount of Ca adsorbed investigated. The behavior of the solid
412 logically follows that of the liquid with lighter values of 1.27 ± 0.23 ‰ (2SE, N=4) (Fig. 3d).
413
414 4.5 Modelling

The results obtained by modelling the experimental Ca adsorption data on δ-MnO_2 by considering two types of sites (i.e. interlayer and edge sites) are shown in Figures 4a and 4b. Consequently, Ca adsorption on δ-MnO_2 suggests two types of adsorption sites on two different reactive surfaces. Their corresponding modeling parameters are shown in Table 1. These results allow to deduce the relative proportion of the two species of Ca as a function of the initial pH values (Fig. 5). For initial pH values between 2 and 4, this model shows that there is an exchange between Ca^{2+} in solution, and Na^{+} and H^{+} adsorbed. This exchange occurs only through sites of fixed charge (interlayer/basal site due to vacancies in the structure). For initial pH>4, the adsorption of Ca^{2+} is maximal and is distributed for approximately 14% on the edge sites and approximately 86% on/in interlayer sites for charge compensation. For adsorption of Ca^{2+} on edge sites, the best fit is obtained by considering a bidentate coordination (see Fig. 4a) rather than monodentate coordination (results not shown).

Final pH's calculated by the model are also in good agreement with experimental ones measured at stationary state (not shown). This can be illustrated in the Appendix in which a good agreement can be observed by comparing the pH variations (i.e. between the initial Ca solution and the supernatant at the end of the experiment) of both experimental and modelled data sets (see Tables 5 and 6 for the variations). The initial pH and the initial Ca concentrations have been presented on the abscissa for the graphical representations throughout the manuscript, in agreement with representations used in previous studies (e.g. Su et al., 2010; Huang et al, 2017; Yuan et al., 2018; Li et al., 2020; Xu et al., 2020).

Note also that over the pH range considered in this study, Ca is either in dissolved or adsorbed form and is never located in precipitated forms. Calculations performed with VisualMinteq TM version 3.1 software associated with the "thermo.vdb" thermodynamic database (Gustafsson, 2013) indeed showed that all solutions recovered after adsorption and desorption experiments

439 are strongly undersaturated with respect to $Ca(NO_3)_2$, $CaCO_3$, $Ca(MnO_4)_2$ and $Ca_2P_2O_7$ solid
440 phases. Thus, isotopic fractionation due to Ca precipitation in solution can be excluded.
441

442 ## 5. Discussion

443 ### 5.1 Calcium fractionation coefficient $\alpha_{\delta\text{-MnO2-solution}}$

444 The experiments show that the solution is enriched in the heavy isotope ^{44}Ca over time to reach
445 a plateau after 65 min of adsorption (Fig. 1). These results agree with those obtained by using
446 phyllosilicate minerals, for which authors reported that the light ^{40}Ca isotope was preferentially
447 adsorbed on the solid (Brazier et al., 2019). The representation of $\Delta^{44/40}Ca$ versus the fraction
448 of Ca in solution (f) shows that the data follow a straight line (Fig. 6). This implies a
449 fractionation in a closed system at equilibrium between δ-MnO_2 and the corresponding solution
450 of Ca and not by a kinetic fractionation process. At first sight the desorption is slow (Fig. 1a),
451 but it is nevertheless complete after 4 successive sequential extractions with Cohex and 242 h
452 of interactions (Fig. 2), probably because Ca is more strongly retained in the interlayer sites
453 which are more abundant than edge sites (see paragraph 4.5). This behavior tends to indicate
454 that Ca forms exchangeable bonds with the studied manganese oxide.
455 From isotopic signatures of supernatant recovered after the adsorption experiment ($\Delta^{44/40}Ca_{LAA}$)
456 and that of the initial solution ($\Delta^{44/40}Ca_{IS}$), a global isotope fractionation factor (i.e. δ-MnO_2-
457 solution) can be calculated as follows:

458 $$\alpha_{\delta-MnO_{2}-solution} = \frac{\Delta^{44/40}Ca_{IS}+1000}{\Delta^{44/40}Ca_{LAA}+1000} \qquad (11)$$

459 We obtain a fractionation factor $\alpha_{\delta\text{-MnO2-solution}}$ equal to 0.99874 ± 0.00005 (N=5). This value is
460 slightly lower than those obtained during the adsorption of Ca on the muscovite of Tuftane
461 (0.99976) or the montmorillonite Swy-2 (0.99991) due to larger amplitudes of fractionation
462 between the solid and the liquid (see paragraph 5.3). Ikeda et al. (2007) showed that exchange

463 reactions of hydrated Ca^{2+} have a weak associative character, suggesting that Ca is mainly
464 linked to water molecules in the solution, in accord with previous studies (e.g., Koneshan et al.,
465 1998; Jalilehvand et al., 2001). Consequently, since our experiments follow a closed-system
466 equilibrium fractionation process, the ^{44}Ca heavy isotope is mainly concentrated in the aqueous
467 phase having the highest bond force constant (Urey, 1947; Bigeleisen and Mayer, 1947),
468 whereas the light ^{40}Ca isotope is preferentially adsorbed to the reactant (i.e., δ-MnO_2 in our
469 case). Thus, similar to the explanation proposed for ^{40}Ca incorporation in carbonate minerals
470 (Marriott et al., 2004) we suggest that the change from Ca binding to water molecules in
471 solution to the binding of Ca to δ-MnO_2 involves a decrease in bond strength and thus causes
472 light ^{40}Ca isotope enrichment into the solid.
473
474 5.2 Factors controlling adsorption
475 Cations can adsorb on internal and external sites of Mn oxides. For vernadite samples, internal
476 sites (i.e., interlayers) exist due to the deficit of charge in the sheets (vacancies) and lead to
477 adsorption of cations above the sheet or within the interlayer space. Cations can also adsorb on
478 edge sites located on the lateral borders of the δ-MnO_2 sheets (i.e., -OH functional groups).
479 Their reactivity depends on the pH of the medium (Villalobos et al., 2003; Manceau et al., 2007;
480 Grangeon et al., 2008; Sherman and Peacock, 2010; Grangeon et al., 2012; Li et al., 2020). The
481 point of zero charge (PZC) of δ-MnO_2 is between pH values of 1.5 and 3 (Murray, 1974; Tonkin
482 et al., 2004 and references therein), which is consistent with our results. Over the whole range
483 of pH values investigated in this study, adsorption takes place which implies that, the pH_{PZC} of
484 studied δ-MnO_2 is below 2. For pH values lower than 4, there is competition between H^+ and
485 Ca^{2+} for the exchange sites available in the system studied (Fig. 3a). This competition is not
486 significant for pH values above 4 (Fig. 3a). Indeed, as pH increases, the -OH sites at the edge
487 of the sheet deprotonate (their pKa has been estimated to be between pH 6 and 7; Tonkin et al.,

2004; van Genuchten and Pena, 2016), allowing the binding of metal cations such as Ca^{2+} (Morton et al., 2001; Tonkin et al., 2004; Villalobos, 2015; van Genuchten and Pena, 2016). At pH 7, except for the lowest values of initial Ca, amounts of adsorbed Ca and desorbed Na remain rather stable compared to the amount of adsorbed protons which increases with increasing initial Ca concentration (Fig. 3c). Furthermore, for a given concentration, for initial pH values above 4, the final pH stabilizes at approximately 6.3 ± 0.3 (2SE, N=4) (Table 5). Beyond pH 6-7, the edge sites are deprotonated, and a release of H^+ ions at these pH values could suggest that the H^+ were located initially in the interlayer or above the vacant sites.

At pH=7, during the first 5 minutes, the $\Delta^{44/40}Ca$ of the liquid increases rapidly to reach 1.31 ‰, which corresponds to approximately 82% Ca adsorption. After 15 minutes, it decreases to 0.63 ‰, corresponding to approximately 95% adsorption, and then reaches a plateau at 1.26 ‰ beyond 35 minutes and almost 100% adsorption (Table 3, Fig. 1). This could correspond to Ca adsorption on two different types of sites: first in the interlayer, and then on the edge sites, then again in the interlayer. It could also correspond to an effect of interlayer migration of adsorbed Ca ions to edge sites. Based on the results reported in Tables 3 and 5, we can estimate that the signatures of Ca bound to the interlayer are enriched in ^{40}Ca ($\Delta^{44/40}Ca$ equal to -0.43 ‰), while those bound to the edge sites are enriched in ^{44}Ca ($\Delta^{44/40}Ca$ equal to 3.5 ‰) (see explanations in Appendix A). At first sight these two splitting intensities might be contradictory to the discussion in section 5.1. However, in section 5.1, we discussed the global average isotope fractionation factor which results from the combination of the apparent isotopic signatures due to adsorption in/on different adsorption sites, as in interlayer space and on the edges (see e.g. Tertre et al., 2009; Lu et al., 2014 for additivity of sorption properties of different types of sorption sites).

5.3 Fractionation amplitude during Ca adsorption on phyllominerals

In this study, a higher amplitude of $\Delta^{44/40}Ca$ fractionation between final and initial solutions during Ca adsorption on δ-MnO_2 (1.19‰) was measured and compared to other minerals previously analyzed in the literature (phyllosilicates; between 0 and 0.22‰) (Brazier et al., 2019). Different fractionation amplitudes were already suggested for different adsorption sites (interlayer or edge sites, as in this study) or for different minerals containing Ca in their crystal lattice (silicates, carbonates, phosphates, hydrous minerals...) or aqueous species. Previous works explained that these different fractionation amplitudes could be related to the coordination number or the mineral-dependent Ca-O bond length (e.g., Hedwig et al., 1980; Katz et al., 1996; Jalilehvand et al., 2001; Ikeda et al., 2007; Colla et al., 2013; Moynier and Fuji, 2017; Huang et al., 2019; Méheut et al., 2021; Nelson et al., 2021). For the adsorption of Ca on phyllosilicate minerals, Brazier et al. (2019) showed that the magnitude of the apparent fractionation of Ca was controlled by the layer charge and the external specific surface of the mineral (i.e., size fraction) considered, as well as by the presence or absence of an interlayer space open to aqueous cations. Following the results of the present study, it can be proposed that the fractionation amplitude depends also on the nature of the site involved in the adsorption (interlayer vs. edge sites; see Section 5.2) and thus on the nature of the bonds. Indeed, the results from the surface complexation model suggest that the adsorption bonds with the edges are of the bidendate type, while those implying interlayer sites create H-bonds between H_2O bound to Ca and O of the sheet (Gaillot, 2002).

Further structural studies are necessary to better explain the mechanisms of fractionation depending on the nature of the adsorption sites involved.

5.4 Conventional methods of extracting bioavailable Ca and implication for natural environments

Identifying nutrient pools and accurately quantifying their size are necessary for the sustainable management of forest ecosystems. Classically, exchangeable reservoirs are considered as major contributors in nutrient cycles in soils. Decomposition of litter, atmospheric inputs and rock/mineral weathering provide nutrient cations, while root removal and runoff via gravity water carry them out of the reservoir. The cations (such as Ca^{2+}, Mg^{2+}, Na^{+}) electrostatically retained on the negative charges of the soil constituents (e.g., humic substances, phyllosilicates, oxy-hydroxides) by outer sphere complexes are generally easily exchangeable with other cations (e.g., Gangloff et al., 2016).

The reserves of basic cations in soils are classically estimated by measuring the quantities of cations extracted by soluble salts (e.g., ammonium acetate, sodium acetate, magnesium chloride, magnesium nitrate, potassium nitrate, ammonium chloride, barium chloride, cobalt hexamine chloride (e.g., Tessier et al., 1979; Ciesielski et al., 1997; Leleyter and Probst, 1999; Blum et al., 2002; Nezat et al., 2007; Holmden and Bélanger, 2010; Bélanger et al., 2012; Moore et al., 2013; Andrews et al., 2016; Bullen and Chadwick, 2016; Lehn et al., 2017). Note, however, that several authors showed that the choice of the salt used for the extraction, as well as the concentration of the salt, pH and interaction times (from 1 h to 24 h), could induce significant variation in the amount of cations that could be exchanged (e.g., Ciesielski et al., 1997; Jaremko and Kalembasa, 2014). The results obtained in the present study showed that the isotopic signature of the solution after Ca desorption from δ-MnO_2 by using a specific desorbent (Cohex) was highly dependent on the concentration of this desorbent and the time of the interaction. Indeed, solution after partial desorption (lower than ~70 % of Ca desorbed) was enriched in heavier isotopes (i.e., positive $\Delta^{44/40}$Ca value in Fig. 2b) compared to the initial solution, while it was enriched in lighter isotopes (i.e., negative $\Delta^{44/40}$Ca value in Fig. 2b) when

562 more than 70% of the Ca is desorbed. In agreement with what we observed for the adsorption
563 experiments, one could suggest that desorption occurs first from a ^{44}Ca-enriched site and then
564 from a ^{40}Ca-enriched site. However, if we make the analogy that, as for the phyllosilicates, Ca
565 desorbs first from the interlayer sites and then from the edges, this is in contradiction with the
566 results of this study, which suggest that the edges have a signature enriched in the heavy isotope
567 (^{44}Ca). Meanwhile, the interlayer space has a signature enriched in the light isotope ^{40}Ca.. Such
568 behavior obtained for δ-MnO_2 is significantly different from what was recently measured from
569 clay minerals (Brazier et al., 2019), especially for smectites and fine muscovite particles, for
570 which isotopic signatures of the desorbed Ca solutions (from Cohex asused in this study) were
571 instantaneously equal to that of the initial solution used to perform adsorption, due to full
572 desorption, irrespective of the time contact. These different behaviors between clay minerals
573 and δ-MnO_2 could be tentatively assigned to structural control during the exchange of Ca^{2+} in
574 the interlayer space of δ-MnO_2 considering other cations (Cohex, K^+ or NH_4^+; Table 4 and Fig.
575 2). Indeed, for Mn oxides, a possible rearrangement of the different cations in the interlayer
576 space during exchange cannot be excluded; a process which could lead to a decrease in the
577 thickness of the interlayer space and can cause then cause a partial collapse of the interlayer as
578 reported in previous studies (Drits et al., 1998; Gaillot, 2002, Han et al., 2022). Furthermore, it
579 is interesting to note that the concentration of aqueous K^+ in natural waters is generally lower
580 than 10^{-2} mol/L (e.g., Wang et al. 2021) implying that desorption of an initial cation adsorbed
581 on mineral (as Ca^{2+} on δ-MnO_2) by another cation in the fluid (as K^+) is rarely total. This leads
582 then to isotopic signature of the fluid after interaction that are highly dependent on the Ca
583 fraction desorbed from the solid. In this context, it is likely that a part of the Ca trapped in the
584 interlayer space will tend not to be desorbed without a weathering reaction leading to hydrolysis
585 of δ-MnO_2. This suggests that under natural condition, not all the bioavailable Ca in soils is
586 attainable by exchange reactions, as often suggested.

587 Finally, other studies have questioned the relevance of using these salts to access the
588 bioavailable fraction of nutrient cations in soils (e.g., Mengel and Rahmatullah, 1994; Hamburg
589 et al., 2003; Lucash et al., 2012). Indeed, different reservoirs that can play a role as Ca reservoirs
590 in soils are not extractable by soluble salts, such as Ca trapped in oxalate compounds, microbial
591 biomass, carbonate minerals, primary minerals (e.g., apatite or secondary minerals, such as Fe
592 oxy-hydroxides) and organic complexes bound in P fractions (Sparks, 1987; Farkas et al., 2011;
593 Dauer and Perakis, 2014; van der Heijden et al., 2014; Schmitt et al., 2017; Chabaux et al.,
594 2019; Rodionov et al., 2020; Uhlig et al., 2020). To extract bioavailable nutrients from these
595 different reservoirs, sequential leaching can be considered. Problems similar to those noted in
596 this study are therefore likely to arise depending on the different reagents/interaction times used
597 in these steps, as well as on the nature of the soil. Combining these basic approaches with
598 isotopic measurements allows us to identify the underlying mechanisms.
599

600 ## 5 Conclusion

601 This study confirms that, as observed for Ca adsorption on phyllosilicates, the light isotope ^{40}Ca
602 is preferentially adsorbed on δ-MnO_2. As the experiments follow equilibrium fractionation in a
603 closed system, this implies that the heavy isotope ^{44}Ca remains preferentially bound to the
604 aqueous phase of the nutrient solution. Our results suggest that at pH below 4, Ca almost
605 exclusively occupies the interlayer space, while above pH 4, Ca first fills the interlayer space
606 (~86%) and then edges (~14%). Our results propose that the isotopic signature of Ca bound to
607 the edge sites is enriched in ^{44}Ca ($\Delta^{44/40}Ca$ equal to 3.5‰) compared to that of Ca adsorbed in
608 the interlayer space ($\Delta^{44/40}Ca$ equal to -0.43‰).
609 This contrasting behavior between the two types of adsorption sites could be due to the
610 bidendate nature of the Ca surface complex formed on the edge sites and to exchange of Ca^{2+}
611 with H^+ in the interlayer sites, as revealed by surface complexation modeling. Finally, our study

612 shows that Ca adsorption on a poorly crystallized phyllomanganate (δ-MnO_2) exhibits the
613 highest fractionation intensity observed to date in Ca adsorption on solids ($\Delta^{44/40}$Ca is equal to
614 1.19 ± 0.15‰). These inter- and intramineral differences could be explained by different types
615 of Ca binding or coordination, with the precise mechanisms yet to be determined.
616 We also observed that, unlike phyllosilicates, the Ca desorption was complete, but not
617 instantaneous. This could be explained by structural control during the exchange of Ca^{2+} in the
618 interlayer, which can lead to the partial collapse of the latter, making Ca difficult to extract.
619 This questions the use of salts in the laboratory and the representativeness of the exchange
620 complex to have access to the full amount of bioavailable Ca. Similarly, in the natural
621 environment, this suggests that other Ca reservoirs should be considered, and that much of
622 bioavailable Ca remains non-extractable using conventional methods.
623

624 **Acknowledgments**

625 This project received financial support from CNRS through the MITI interdisciplinary ISOTOP
626 program. Colin Fourtet from ITES is acknowledged for his help with elementary concentration
627 measurements. Eric Pelt, also from ITES, is thanked for his help with Triton. Jean-Dominique
628 Comparot from IC2MP is thanked for specific surface area measurements. AD Schmitt wants
629 to thank Merlin Méheut for discussion about mechanisms governing isotopic fractionations.
630 The manuscript benefitted from constructive reviews by three anonymous reviewers, the
631 executive editor, J. G. Catalano, and the associate editor O. S. Pokrovsky
632

633 **Appendix A. Supplementary Materials**

634 Information about X-ray data performed on the studied δ-MnO_2, comparison of initial and final
635 pH values for experimental and modelled data as well as calculation of $\Delta^{44/40}$Ca isotope
636 signature in the interlayer and on the edges are provided in Supplementary materials.

637 **Bibliography**

638 Andrews M. G., Jacobson A. D., Lehn G. O., Horton T. W. and Craw D. (2016) Radiogenic
639 and stable Sr isotope ratios ($^{87}Sr/^{86}Sr$, $\delta^{88}/^{86}Sr$) as tracers of riverine cation sources and
640 biogeochemical cycling in the Milford Sound region of Fiordland, New Zealand.
641 *Geochim. Cosmochim. Acta* 173, 284–303.

642 Bagard M.-L., Schmitt A.-D., Chabaux F., Pokrovsky O. S., Viers J., Stille P., Labolle F. and
643 Prokushkin A. S. (2013) Biogeochemistry of stable Ca and radiogenic Sr isotopes in a
644 larch-covered permafrost-dominated watershed of Central Siberia. *Geochim.*
645 *Cosmochim. Acta* 114, 169–187.

646 Baize D. (1997) *Teneurs totales en éléments traces métalliques dans les sols (france)*. INRA
647 Editions, Versailles.

648 Balistrieri L. S. and Murray J. W. (1982) The surface chemistry of δMnO_2 in major ion sea
649 water. *Geochim. Cosmochim. Acta* 46, 1041–1052.

650 Bélanger N., Holmden C., Courchesne F., Côté B. and Hendershot W. H. (2012) Constraining
651 soil mineral weathering $^{87}Sr/^{86}Sr$ for calcium apportionment studies of a deciduous forest
652 growing on soils developed from granitoid igneous rocks. *Geoderma* 185–186, 84–96.

653 Bigeleisen J. and Mayer M. G. (1947) Calculation of Equilibrium Constants for Isotopic
654 Exchange Reactions. *J. Chem. Phys.* 15, 261–267.

655 Black J. R., Epstein E., Rains W. D., Yin Q. and Casey W. H. (2008) Magnesium-Isotope
656 Fractionation During Plant Growth. *Environ. Sci. Technol*. 42, 7831–7836.

657 Blum J. D., Klaue A., Nezat C. A., Driscoll C. T., Johnson C. E., Siccama T. G., Eagar C.,
658 Fahey T. J. and Likens G. E. (2002) Mycorrhizal weathering of apatite as an important
659 calcium source in base-poor forest ecosystems. *Nature* 417, 729–731.

660 Bradbury M. H. and Baeyens B. (2009) Sorption modelling on illite Part I: Titration
661 measurements and the sorption of Ni, Co, Eu and Sn. *Geochim. Cosmochim. Acta* 73,
662 990–1003.

663 Brazier J.-M., Schmitt A.-D., Gangloff S., Pelt E., Chabaux F. and Tertre E. (2019) Calcium
664 isotopic fractionation during adsorption onto and desorption from soil phyllosilicates
665 (kaolinite, montmorillonite and muscovite). *Geochim. Cosmochim. Acta* 250, 324–347.

666 Brazier J.-M., Schmitt A.-D., Gangloff S., Pelt E., Gocke M. I. and Wiesenberg G. L. B. (2020)
667 Multi-isotope approach ($\delta^{44/40}Ca$, $\delta^{88/86}Sr$ and $^{87}Sr/^{86}Sr$) provides insights into rhizolith
668 formation mechanisms in terrestrial sediments of Nussloch (Germany). *Chem. Geol.* 545,
669 119641.

670 Brunauer S., Emmett P. H. and Teller E. (1938) Adsorption of Gases in Multimolecular Layers.
671 *J. Am. Chem. Soc.* 60, 309–319.

672 Bullen T. and Chadwick O. (2016) Ca, Sr and Ba stable isotopes reveal the fate of soil nutrients
673 along a tropical climosequence in Hawaii. *Chem. Geol.* 422, 25–45.

674 Burdige D. J., Dhakar S. P. and Nealson K. H. (1992) Effects of manganese oxide mineralogy
675 on microbial and chemical manganese reduction. *Geomicrobiol. J.* 10, 27–48.

676 Burns R. G. and Burns V. M. (1977) Chapter 7 Mineralogy. In *Elsevier Oceanography Series*
677 (ed. G. P. Glasby). Marine Manganese Deposits. Elsevier. pp. 185–248.

678 Catts J. G. and Langmuir D. (1986) Adsorption of Cu, Pb and Zn by δMnO_2: applicability of
679 the site binding-surface complexation model. *Appl. Geochem.*1, 255–264.

680 Cenki-Tok B., Chabaux F., Lemarchand D., Schmitt A.-D., Pierret M.-C., Viville D., Bagard
681 M.-L. and Stille P. (2009) The impact of water–rock interaction and vegetation on
682 calcium isotope fractionation in soil- and stream waters of a small, forested catchment
683 (the Strengbach case). *Geochim. Cosmochim. Acta* 73, 2215–2228.

684 Chabaux F., Stille P., Prunier J., Gangloff S., Lemarchand D., Morvan G., Négrel J., Pelt E.,
685 Pierret M.-C., Rihs S., Schmitt A.-D., Trémolières M. and Viville D. (2019) Plant-soil-
686 water interactions: Implications from U-Th-Ra isotope analysis in soils, soil solutions and
687 vegetation (Strengbach CZO, France). *Geochim. Cosmochim. Acta* 259, 188–210.

688 Ciesielski H., Sterckeman T., Santerne M. and Willery J. P. (1997) Determination of cation
689 exchange capacity and exchangeable cations in soils by means of cobalt hexamine
690 trichloride. Effects of experimental conditions. *Agronomie* 17, 1–7.

691 Cobert F., Schmitt A.-D., Bourgeade P., Labolle F., Badot P.-M., Chabaux F. and Stille P.
692 (2011) Experimental identification of Ca isotopic fractionations in higher plants.
693 *Geochim. Cosmochim. Acta* 75, 5467–5482.

694 Colla C. A., Wimpenny J., Yin Q.-Z., Rustad J. R. and Casey W. H. (2013) Calcium-isotope
695 fractionation between solution and solids with six, seven or eight oxygens bound to
696 Ca(II). *Geochim. Cosmochim. Acta* 121, 363–373.

697 Dauer J. M. and Perakis S. S. (2014) Calcium oxalate contribution to calcium cycling in forests
698 of contrasting nutrient status. *For. Ecol. Manage.* 334, 64–73.

699 Dorn R. I., Krinsley D. H., Liu T., Anderson S., Clark J., Cahill T. A. and Gill T. E. (1992)
700 Manganese-rich rock varnish does occur in Antarctica. *Chem. Geol.* 99, 289–298.

701 Drits V. A., Lanson B., Gorshkov A. I. and Manceau A. (1998) Substructure and superstructure
702 of four-layer Ca-exchanged birnessite. *Am. Mineral.* 83, 97–118.

703 Drits V. A., Silvester E., Gorshkov A. I. and Manceau A. (1997) Structure of synthetic
704 monoclinic Na-rich birnessite and hexagonal birnessite: I. Results from X-ray diffraction
705 and selected-area electron diffraction. *Am. Mineral.* 82, 946–961.

706 Eisenhauer A., Nägler T. F., Stille P., Kramers J., Gussone N., Bock B., Fietzke J., Hippler D.
707 and Schmitt A.-D. (2004) Proposal for International Agreement on Ca Notation Resulting
708 from Discussions at Workshops on Stable Isotope Measurements Held in Davos
709 (Goldschmidt 2002) and Nice (EGS-AGU-EUG 2003). *Geostand. Geoanal. Res.* 28,
710 149–151.

711 Farkaš J., Déjeant A., Novák M. and Jacobsen S. B. (2011) Calcium isotope constraints on the
712 uptake and sources of Ca^{2+} in a base-poor forest: A new concept of combining stable
713 ($\delta^{44/42}$Ca) and radiogenic (εCa) signals. *Geochim. Cosmochim. Acta* 75, 7031–7046.

714 Gaillot A.-C. (2002) Caractérisation structurale de la birnessite : Influence du protocole de
715 synthèse. Phd-thesis, Université Joseph-Fourier - Grenoble I.

716 Gaines G. L. and Thomas H. C. (1953) Adsorption Studies on Clay Minerals. II. A Formulation
717 of the Thermodynamics of Exchange Adsorption. *J. Chem. Phys.* 21, 714–718.

718 Gangloff S., Stille P., Pierret M.-C., Weber T. and Chabaux F. (2014) Characterization and
719 evolution of dissolved organic matter in acidic forest soil and its impact on the mobility

of major and trace elements (case of the Strengbach watershed). *Geochim. Cosmochim. Acta* 130, 21–41.

Gangloff S., Stille P., Schmitt A.-D. and Chabaux F. (2016) Factors controlling the chemical composition of colloidal and dissolved fractions in soil solutions and the mobility of trace elements in soils. *Geochim. Cosmochim. Acta* 189, 37–57.

van Genuchten C. M. and Peña J. (2016) Sorption selectivity of birnessite particle edges: a d-PDF analysis of Cd(II) and Pb(II) sorption by δ-MnO_2 and ferrihydrite. *Environ. Sci. Process Impacts* 18, 1030–1041.

Godtfredsen K. L. and Stone A. T. (1994) Solubilization of manganese dioxide-bound copper by naturally occurring organic compounds. *Environ. Sci. Technol.* 28, 1450–1458.

Grangeon S., Fernandez-Martinez A., Claret F., Marty N., Tournassat C., Warmont F. and Gloter A. (2017) In-situ determination of the kinetics and mechanisms of nickel adsorption by nanocrystalline vernadite. *Chem. Geol.* 459, 24–31.

Grangeon S., Lanson B., Lanson M. and Manceau A. (2008) Crystal structure of Ni-sorbed synthetic vernadite: a powder X-ray diffraction study. *Mineral. Mag.* 72, 1279–1291.

Grangeon S., Manceau A., Guilhermet J., Gaillot A.-C., Lanson M. and Lanson B. (2012) Zn sorption modifies dynamically the layer and interlayer structure of vernadite. *Geochim. Cosmochim. Acta* 85, 302–313.

Griffith E. M., Schmitt A.-D., Andrews M. G. and Fantle M. S. (2020) Elucidating modern geochemical cycles at local, regional, and global scales using calcium isotopes. *Chem. Geol.* 534, 119445.

Gustafsson J. P. (2013) *Visual MINTEQ. Version 3.1.*, Division of Land and Water Resources. Royal Institute of Technology, Stockholm, Sweden.

Hamburg S. P., Yanai R. D., Arthur M. A., Blum J. D. and Siccama T. G. (2003) Biotic Control of Calcium Cycling in Northern Hardwood Forests: Acid Rain and Aging Forests. *Ecosystems* 6, 399–406.

Han S. and Kwon K. D. (2022) Interlayer water structure of phyllomanganates: Insights from MD simulations of chalcophanite-group oxide dehydration. *Geochim. Cosmochim. Acta* 318, 495–509.

Hedwig G. R., Liddle J. R. and Reeves R. D. (1980) Complex formation of nickel(II) ions with citric acid in aqueous solution: a potentiometric and spectroscopic study. *Aust. J. Chem.* 33, 1685–1693.

van der Heijden G., Legout A., Pollier B., Ranger J. and Dambrine E. (2014) The dynamics of calcium and magnesium inputs by throughfall in a forest ecosystem on base poor soil are very slow and conservative: evidence from an isotopic tracing experiment (^{26}Mg and ^{44}Ca). *Biogeochemistry* 118, 413–442.

Heuser A., Schmitt A.-D., Gussone N., Wombacher F. (2016) Analytical methods. In: Gussone N., Schmitt A.-D., Heuser A., Wombacher F., Dietzel M., Tipper E., Schiller M. "Calcium Stable Isotope Geochemistry", Springer, 23-73.

Hippler D., Schmitt A.-D., Gussone N., Heuser A., Stille P., Eisenhauer A. and Nägler T. F. (2003) Calcium Isotopic Composition of Various Reference Materials and Seawater. *Geostand. newsl.* 27, 13–19.

Holmden C. and Bélanger N. (2010) Ca isotope cycling in a forested ecosystem. *Geochim. Cosmochim. Acta* 74, 995–1015.

Huang F., Zhou C., Wang W., Kang J. and Wu Z. (2019) First-principles calculations of equilibrium Ca isotope fractionation: Implications for oldhamite formation and evolution of lunar magma ocean. *Earth Planet. Sci. Lett.* 510, 153–160.

Huang X., Chen T., Zou X., Zhu M., Chen D. and Pan M. (2017) The Adsorption of Cd(II) on Manganese Oxide Investigated by Batch and Modeling Techniques. *IJERPH* 14, 1145.

Ikeda T., Nishiyama T., Yamada S. and Yanagi T. (2007) Microstructures of olivine-plagioclase corona in meta-ultramafic rocks from Sefuri Mountains, NW Kyushu, Japan. *Lithos* 97, 289–306.

Jalilehvand F., Spångberg D., Lindqvist-Reis P., Hermansson K., Persson I. and Sandström M. (2001) Hydration of the Calcium Ion. An EXAFS, Large-Angle X-ray Scattering, and Molecular Dynamics Simulation Study. *J. Am. Chem. Soc.* 123, 431–441.

Jaremko D. and Kalembasa D. (2014) A Comparison of Methods for the Determination of Cation Exchange Capacity of Soils/Porównanie Metod Oznaczania Pojemności Wymiany Kationów I Sumy Kationów Wymiennych W Glebach. *Ecol. Chem. Eng. S* 21, 487–498.

Katz A. K., Glusker J. P., Beebe S. A. and Bock C. W. (1996) Calcium Ion Coordination: A Comparison with That of Beryllium, Magnesium, and Zinc. *J. Am. Chem. Soc.* 118, 5752–5763.

Koneshan S., Rasaiah J. C., Lynden-Bell R. M. and Lee S. H. (1998) Solvent Structure, Dynamics, and Ion Mobility in Aqueous Solutions at 25 °C. *J. Phys. Chem. B* 102, 4193–4204.

Lanson B., Drits V. A., Gaillot A.-C., Silvester E., Plançon A. and Manceau A. (2002) Structure of heavy-metal sorbed birnessite: Part 1. Results from X-ray diffraction. *Am. Mineral.* 87, 1631–1645.

Lanson B., Drits V. A., Silvester E. and Manceau A. (2000) Structure of H-exchanged hexagonal birnessite and its mechanism of formation from Na-rich monoclinic buserite at low pH. *Am. Mineral.* 85, 826–838.

Lehn G. O., Jacobson A. D., Douglas T. A., McClelland J. W., Barker A. J. and Khosh M. S. (2017) Constraining seasonal active layer dynamics and chemical weathering reactions occurring in North Slope Alaskan watersheds with major ion and isotope (δ^{34}SSO4, δ^{13}CDIC, $^{87}Sr/^{86}Sr$, $\delta^{44/40}$Ca, and $\delta^{44/42}$Ca) measurements. *Geochim. Cosmochim. Acta* 217, 399–420.

Lehn G. O., Jacobson A. D. and Holmden C. (2013) Precise analysis of Ca isotope ratios (δ44/40Ca) using an optimized ^{43}Ca–^{42}Ca double-spike MC-TIMS method. *Int. J. Mass Spectrom.* 351, 69–75.

Leleyter L. and Probst J.-L. (1999) A New Sequential Extraction Procedure for the Speciation of Particulate Trace Elements in River Sediments. *Int. J. Environ. Anal. Chem.* 73, 109–128.

Li Y., Zhao X., Wu J. and Gu X. (2020) Surface complexation modeling of divalent metal cation adsorption on birnessite. *Chem. Geol.* 551, 119774.

Lucash M. S., Yanai R. D., Blum J. D. and Park B. B. (2012) Foliar Nutrient Concentrations Related to Soil Sources across a Range of Sites in the Northeastern United States. *Soil Sci. Soc. Am. J.* 76, 674–683.

Lu J., Tertre E. and Beaucaire C. (2014) Assesment of a predictive model to describe the migration of major inorganic cations in a Bt soil horizon. *Appl. Geochem.* 41, 151-162.

Luo J., Zhang Q. and Suib S. L. (2000) Mechanistic and Kinetic Studies of Crystallization of Birnessite. *Inorg. Chem.* 39, 741–747.

Manceau A., Lanson M. and Geoffroy N. (2007) Natural speciation of Ni, Zn, Ba, and As in ferromanganese coatings on quartz using X-ray fluorescence, absorption, and diffraction. *Geochim. Cosmochim. Acta* 71, 95–128.

Manceau A., Marcus M. A., Grangeon S., Lanson M., Lanson B., Gaillot A.-C., Skanthakumar S. and Soderholm L. (2013) Short-range and long-range order of phyllomanganate nanoparticles determined using high-energy X-ray scattering. *J. Appl. Crystallogr.* 46, 193–209.

Marafatto F. F., Lanson B. and Peña J. (2018) Crystal growth and aggregation in suspensions of δ-MnO_2 nanoparticles: implications for surface reactivity. *Environ. Sci.: Nano* 5, 497–508.

Marriott C. S., Henderson G. M., Belshaw N. S. and Tudhope A. W. (2004) Temperature dependence of δ7Li, δ^{44}Ca and Li/Ca during growth of calcium carbonate. *Earth Planet. Sci. Lett.* 222, 615–624.

Marschner H. (1995) Mineral nutrition of higher plants 2nd Ed. *Institute of Plant Nutrition University of Hohenheim: Germany*.

Mengel K. and Rahmatullah (1994) Exploitation of potassium by various crop species from primary minerals in soils rich in micas. *Biol. Fertil. Soils* 17, 75–79.

Moore J., Jacobson A. D., Holmden C. and Craw D. (2013) Tracking the relationship between mountain uplift, silicate weathering, and long-term CO_2 consumption with Ca isotopes: Southern Alps, New Zealand. *Chem. Geol.* 341, 110–127.

Morton J. D., Semrau J. D. and Hayes K. F. (2001) An X-ray absorption spectroscopy study of the structure and reversibility of copper adsorbed to montmorillonite clay. *Geochim. Cosmochim. Acta* 65, 2709–2722.

Moynier F. and Fujii T. (2017) Calcium isotope fractionation between aqueous compounds relevant to low-temperature geochemistry, biology and medicine. *Sci. Rep.* 7, 44255.

Murray J. W. (1975) The interaction of metal ions at the manganese dioxide-solution interface. *Geochim. Cosmochim. Acta* 39, 505–519.

Murray J. W. (1974) The surface chemistry of hydrous manganese dioxide. *J. Colloid Interface Sci.* 46, 357–371.

Nelson C. J., Jacobson A. D., Kitch G. D. and Weisenberger T. B. (2021) Large calcium isotope fractionations by zeolite minerals from Iceland. *Commun. Earth Environ.* 2, 1–12.

Nelson Y. M., Lion L. W., Ghiorse W. C. and Shuler M. L. (1999) Production of Biogenic Mn Oxides by *Leptothrix discophora* SS-1 in a Chemically Defined Growth Medium and Evaluation of Their Pb Adsorption Characteristics. *Appl. Environ. Microbiol.* 65, 175–180.

Nezat C. A., Blum J. D., Yanai R. D. and Hamburg S. P. (2007) A sequential extraction to determine the distribution of apatite in granitoid soil mineral pools with application to weathering at the Hubbard Brook Experimental Forest, NH, USA. *Appl. Geochem.* 22, 2406–2421.

Palumbo B., Bellanca A., Neri R. and Roe M. J. (2001) Trace metal partitioning in Fe–Mn nodules from Sicilian soils, Italy. *Chem. Geol.* 173, 257–269.

Peña J., Bargar J. R. and Sposito G. (2015) Copper sorption by the edge surfaces of synthetic birnessite nanoparticles. *Chem. Geol.* 396, 196–207.

Post J. E. and Veblen D. R. (1990) Crystal structure determinations of synthetic sodium, magnesium, and potassium birnessite using TEM and the Rietveld method. *Am. Mineral.* 75, 477–489.

Reinholdt M. X., Hubert F., Faurel M., Tertre E., Razafitianamaharavo A., Francius G., Prêt D., Petit S., Béré E., Pelletier M. and Ferrage E. (2013) Morphological properties of vermiculite particles in size-selected fractions obtained by sonication. *Appl. Clay Sci.* 77–78, 18–32.

Rodionov A., Bauke S. L., von Sperber C., Hoeschen C., Kandeler E., Kruse J., Lewandowski H., Marhan S., Mueller C. W., Simon M., Tamburini F., Uhlig D., von Blanckenburg F., Lang F. and Amelung W. (2020) Biogeochemical cycling of phosphorus in subsoils of temperate forest ecosystems. *Biogeochemistry* 150, 313–328.

Schmitt A.-D. (2016) Earth-Surface Ca Isotopic Fractionations. In *Calcium Stable Isotope Geochemistry* Advances in Isotope Geochemistry. Springer Berlin Heidelberg, Berlin, Heidelberg. pp. 145–172.

Schmitt A.-D., Borrelli N., Ertlen D., Gangloff S., Chabaux F. and Osterrieth M. (2018) Stable calcium isotope speciation and calcium oxalate production within beech tree (Fagus sylvatica L.) organs. *Biogeochemistry* 137, 197–217.

Schmitt A.-D., Cobert F., Bourgeade P., Ertlen D., Labolle F., Gangloff S., Badot P.-M., Chabaux F. and Stille P. (2013) Calcium isotope fractionation during plant growth under a limited nutrient supply. *Geochim. Cosmochim. Acta* 110, 70–83.

Schmitt A.-D., Gangloff S., Labolle F., Chabaux F. and Stille P. (2017) Calcium biogeochemical cycle at the beech tree-soil solution interface from the Strengbach CZO (NE France): insights from stable Ca and radiogenic Sr isotopes. *Geochim. Cosmochim. Acta* 213, 91–109.

Schmitt A.-D., Vigier N., Lemarchand D., Millot R., Stille P. and Chabaux F. (2012) Processes controlling the stable isotope compositions of Li, B, Mg and Ca in plants, soils and waters: A review. *C. R. Geosci.* 344, 704–722.

Sherman D. M. and Peacock C. L. (2010) Surface complexation of Cu on birnessite (δ-MnO_2): Controls on Cu in the deep ocean. *Geochim. Cosmochim. Acta* 74, 6721–6730.

Simanova A. A., Kwon K. D., Bone S. E., Bargar J. R., Refson K., Sposito G. and Peña J. (2015) Probing the sorption reactivity of the edge surfaces in birnessite nanoparticles using nickel(II). *Geochim. Cosmochim. Acta* 164, 191–204.

Sparks D. L. (1987) Potassium Dynamics in Soils. In *Advances in Soil Science* (ed. B. A. Stewart). Advances in Soil Science. Springer, New York, NY. pp. 1–63.

887 Su Q., Pan B., Wan S., Zhang W. and Lv L. (2010) Use of hydrous manganese dioxide as a
888 potential sorbent for selective removal of lead, cadmium, and zinc ions from water. *J.*
889 *Colloid Interface Sci.* 349, 607–612.

890 Tertre E., Prêt D. and Ferrage E. (2011) Influence of the ionic strength and solid/solution ratio
891 on Ca(II)-for-Na^+ exchange on montmorillonite. Part 1: Chemical measurements,
892 thermodynamic modeling and potential implications for trace elements geochemistry. *J.*
893 *Colloid Interface Sci.* 353, 248–256.

894 Tertre E. Beaucaire C., Coreau N. and Juery A. (2009) Modeling of Zn sorption onto clayey
895 sediments using a multi-site and multi-component ion-exchange model. *Appl. Geochem.*
896 24, 1852-1861.

897 Tessier A., Campbell P. G. C. and Bisson M. (1979) Sequential extraction procedure for the
898 speciation of particulate trace metals. *Anal. Chem.* 51, 844–851.

899 Tonkin J. W., Balistrieri L. S. and Murray J. W. (2004) Modeling sorption of divalent metal
900 cations on hydrous manganese oxide using the diffuse double layer model. *Appl.*
901 *Geochem.* 19, 29–53.

902 Uhlig D., Amelung W. and von Blanckenburg F. (2020) Mineral Nutrients Sourced in Deep
903 Regolith Sustain Long-Term Nutrition of Mountainous Temperate Forest Ecosystems.
904 *Global Biogeochem. Cycles* 34, 1–21.

905 Urey H. C. (1947) The thermodynamic properties of isotopic substances. *J. Chem. Soc.*
906 *Resumed.* 7, 562–581.

907 Villalobos M. (2015) The Role of Surface Edge Sites in Metal(loid) Sorption to Poorly-
908 Crystalline Birnessites. In *Advances in the Environmental Biogeochemistry of Manganese*
909 *Oxides* ACS Symposium Series. American Chemical Society. pp. 65–87.

910 Villalobos M., Lanson B., Manceau A., Toner B. and Sposito G. (2006) Structural model for
911 the biogenic Mn oxide produced by Pseudomonas putida. *Am. Mineral.* 91, 489–502.

912 Villalobos M., Toner B., Bargar J. and Sposito G. (2003) Characterization of the manganese
913 oxide produced by pseudomonas putida strain MnB1. *Geochim. Cosmochim. Acta* 67,
914 2649–2662.

915 Wang K., Peucker-Ehrenbrink B., Chen H., Lee H. and Hasenmueller E. A. (2021) Dissolved
916 potassium isotopic composition of major world rivers. *Geochim. Cosmochim. Acta* 294,
917 145–159.

918 Xu J., Fan Q., Niu Z., Li Y., Li P. and Wu W. (2012) Studies of Eu(III) sorption on TiO2:
919 Effects of pH, humic acid and poly(acrylic acid). *Chem. Eng. J.* 179, 186–192.

920 Yuan W., Saldi G. D., Chen J., Vetuschi Zuccolini M., Birck J.-L., Liu Y. and Schott J.
921 (2018) Gallium isotope fractionation during Ga adsorption on calcite and goethite.
922 *Geochim. Cosmochim. Acta* 223, 350–363.

923 Zhao W., Feng X., Tan W., Liu F. and Ding S. (2009) Relation of lead adsorption on birnessites
924 with different average oxidation states of manganese and release of $Mn^{2+}/H^+/K^+$. *J.*
925 *Environ. Sci.* 21, 520–526.

926

927

928 **Table captions**

929

930 **Table 1:** Parameters of the surface complexation model used to interpret Ca adsorption on δ-
931 MnO_2 (E_i: equivalent fraction in charge of the CEC occupied by the "i" species (eq/eq), {i}:
932 activity of the aqueous species "i", F: Faraday constant 96485 C/mol, R: ideal gas constant
933 8.314 J/mol/.K, T: temperature in K, φo : surface potential (V) in the surface plane (O – plane)
934 and see section 3 in the text for details). * from Tonkin et al. (2004) and Van Guenuchten et
935 Peña (2016), ** optimized values, determined by PEST option, allowing to interpret
936 experimental data.

937

938 **Table 2:** Characteristics of studied δ-MnO_2 mineral and maximum amount of adsorbed Ca and
939 associated $^{44/40}$Ca isotopic fractionation measured in this study. Comparison of data with those
940 previously obtained by Brazier et al. (2019) for clay minerals.

941

942 **Table 3:** Amount of adsorbed Ca and desorbed Na and Ca apparent isotopic fractionation
943 between initial solution and supernatant measured after adsorption using 50 mg of δ-MnO_2 and
944 initial Ca concentration of 0.10 mmol/mmol Mn for variable interaction time steps. LAA=
945 liquid after adsorption, ini = initial, fin = final.

946

947 **Table 4:** Amount of desorbed Ca and Ca apparent isotopic fractionation between initial solution
948 and supernatant after desorption experiments uncorrected and corrected with respect to Ca
949 contributions in residual liquid (clay slurry) and desorbent at pH 7. LAA = liquid after
950 adsorption, LAD = liquid after desorption, ini = initial, LAD_corr = liquid after desorption
951 corrected from slurry and from desorbent Ca contributions.

952

Table 5: Amount of adsorbed Ca and H, desorbed Na and Ca apparent isotopic fractionation between initial solution and supernatant and in solid after adsorption using 50 mg of δ-MnO_2, initial Ca concentration of 0.124 mmol/mmol Mn at variable initial pH values and after 125 min of interaction time. Concentration of adsorbed Ca is calculated as the difference between initial concentration of Ca (i.e., 0.124 mmol/mmol Mn) and concentration of Ca in supernatant after adsorption experiment. Concentration of desorbed Na is calculated from the concentration of Na in solution after adsorption minus the initial concentration of Na (i.e., 0.002 mmol/mmol Mn). LAA= liquid after adsorption, SAA= solid after adsorption, ini = initial, fin = final.

Table 6: Amount of adsorbed Ca and desorbed Na, and Ca apparent isotopic fractionation between initial solution and supernatant and in solid after adsorption using 50 mg of δ-MnO_2 at variable initial Ca concentrations and after 125 min of interaction time. Amount of adsorbed Ca was calculated as the difference between initial amount of Ca and amount of Ca in supernatant after adsorption experiment. Amount of desorbed Na was calculated from the difference between the amount of Na in solution after adsorption and in the initial solution (i.e., 0.002 mmol/mmol Mn). LAA= liquid after adsorption, SAA= solid after adsorption, ini = initial, fin = final, ads = adsorption, des = desorption.

973 **Figure Captions**

974

975 **Fig. 1:** Variation of (a) concentration of Ca and (b) $\Delta^{44/40}$Ca in the liquid after adsorption (LAA)
976 and desorption (LAD) experiments as function of interaction time**.** Experiments were conducted
977 at pH 7 with Ca concentration of 0.1 mmol/mmol Mn. Desorption was performed using 0.1 M
978 Cohex. LAA = liquid after adsorption, LAD = liquid after desorption**.**

979

980 **Fig. 2:** Variation of (a) percentage of Ca adsorbed (the 5% repeatability is comprised within
981 the symbols) and (b) $\Delta^{44/40}$Ca in liquid after desorption with different desorbents at different
982 concentrations and at varying times. IS = initial solution. The weighted average value of the
983 different 0.1 M Cohex extractions is -0.12 ± 0.24 ‰, which is equal, within propagated error,
984 to the value of the initial solution used for the experiments ensuring mass balance comp. This
985 value is represented by the orange straight line, and the error corresponds to the orange dashed
986 lines.

987

988 **Fig. 3:** Variation of: (a) concentrations H+ and Ca^{2+} adsorbed and Na^{+} desorbed as a function
989 of initial pH, (b) $\Delta^{44/40}$Ca in liquid after adsorption (LAA) and solid after adsorption (SAA) as
990 function of initial pH, (c) concentrations H^{+} and Ca^{2+} adsorbed and Na^{+} desorbed as function
991 of initial Ca concentration , and (d) $\Delta^{44/40}$Ca in liquid (LAA) and in solid (SAA) after adsorption
992 as function of initial Ca concentration.
993 For (b) and (d), dotted circles correspond to weighted average isotopic value between LAA and
994 SAA. The dashed line shows that all the values are equal to zero, i.e., similar to that of initial
995 solution, pointing to isotopic mass balance (see text for explanation).

996

997 **Fig. 4**: (a) Amount of Ca^{2+} and H^{+} adsorbed and Na^{+} desorbed as function of initial pH, and
998 (b) Amount of Ca^{2+} and H^{+} adsorbed and Na^{+} desorbed as function of the initial concentration

of Ca (initial pH = 7). Our experimental data are shown with symbols while the SCM results are depicted by dotted lines.

Fig. 5: Percentage of Ca adsorbed on interlayer and edge sites as a function of initial pH

Fig. 6: Evolution of Ca reservoirs in solution and corresponding δ-MnO_2 solid showing $\Delta^{44/40}Ca$ as a function of the fraction of remaining Ca in solution.

The pH variation dataset corresponds to a fixed initial Ca^{2+} concentration of 0.124 mmol/mmol Mn and variable pH values (i.e. $\Delta^{44/40}Ca_{LAA}$ & $\Delta^{44/40}Ca_{SAA}$ from Table 4).

The Conc. variation dataset corresponds to variable Ca^{2+} concentrations and fixed initial pH equal to 7 (i.e. $\Delta^{44/40}Ca_{LAA}$ & $\Delta^{44/40}Ca_{SAA}$ from Table 5).

The Time var. dataset refers to a fixed initial Ca^{2+} concentration of 0.10 mmol/mmol Mn and fixed initial pH equal to 7 for experimental time over 65 min (i.e. $\Delta^{44/40}Ca_{LAA}$ from Table 2)

Kinetic theoretical law was drawn from equation $\partial_{reactant} = [(\partial_{reactant0} + 1000) \times f^{\alpha-1}] - 1000$ (Ding et al., 2005). Equilibrium theoretical law was its part drawn from $\partial_{product} = \alpha \times (\partial_{reactant0} + 1000) \times f^{\alpha-1} \times 1000$ (Black et al., 2008), with α fractionation factor (reactant/product) and f: fraction of Ca remaining in solution.

Fig. 1

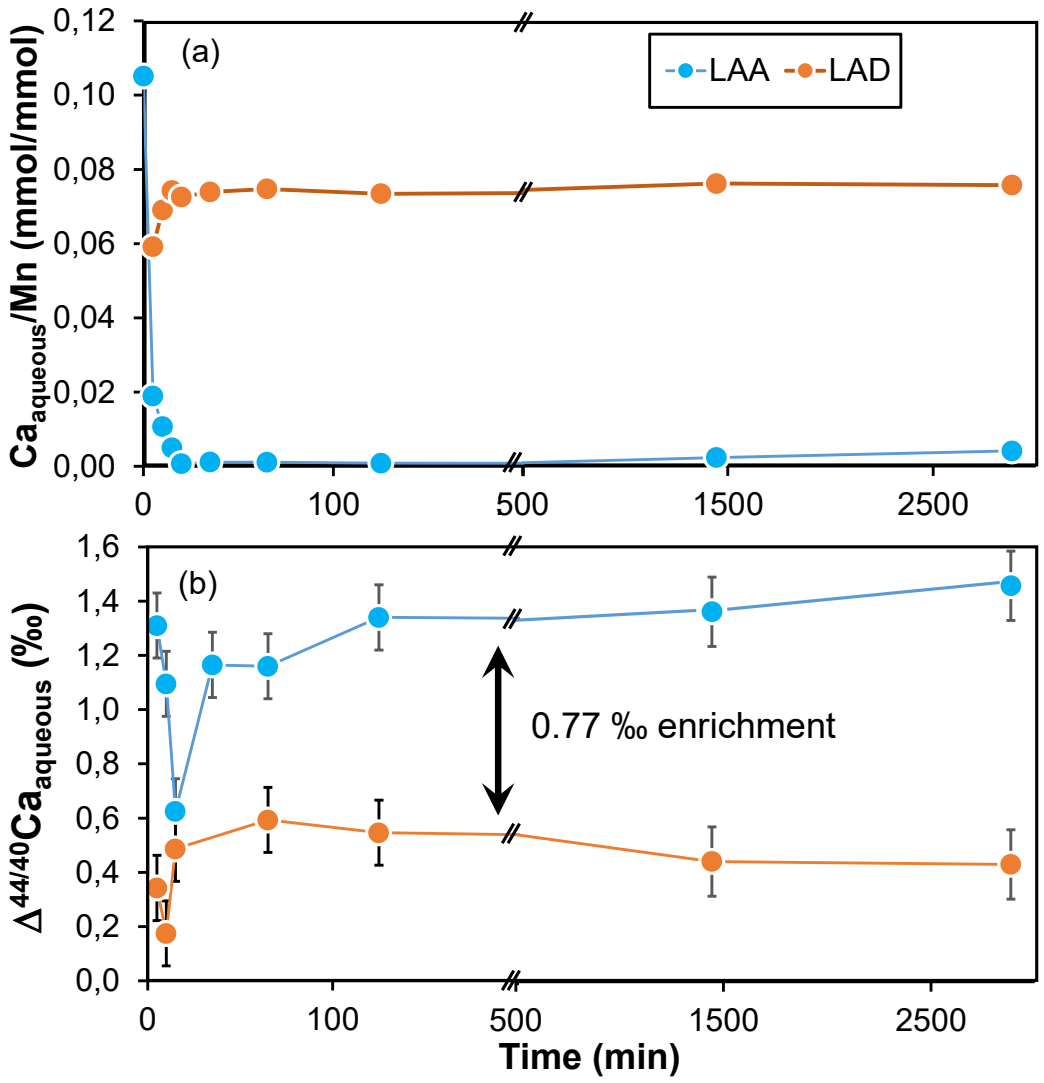
(a)
LAA
LAD
$Ca_{aqueous}$/Mn (mmol/mmol)
0,12
0,10
0,08
0,06
0,04
0,02
0,00
0
100
500
1500
2500
(b)
$\Delta^{44/40}Ca_{aqueous}$ (‰)
1,6
1,4
1,2
1,0
0,8
0,6
0,4
0,2
0,0
0.77 ‰ enrichment
Time (min)

1035 **Fig. 2**

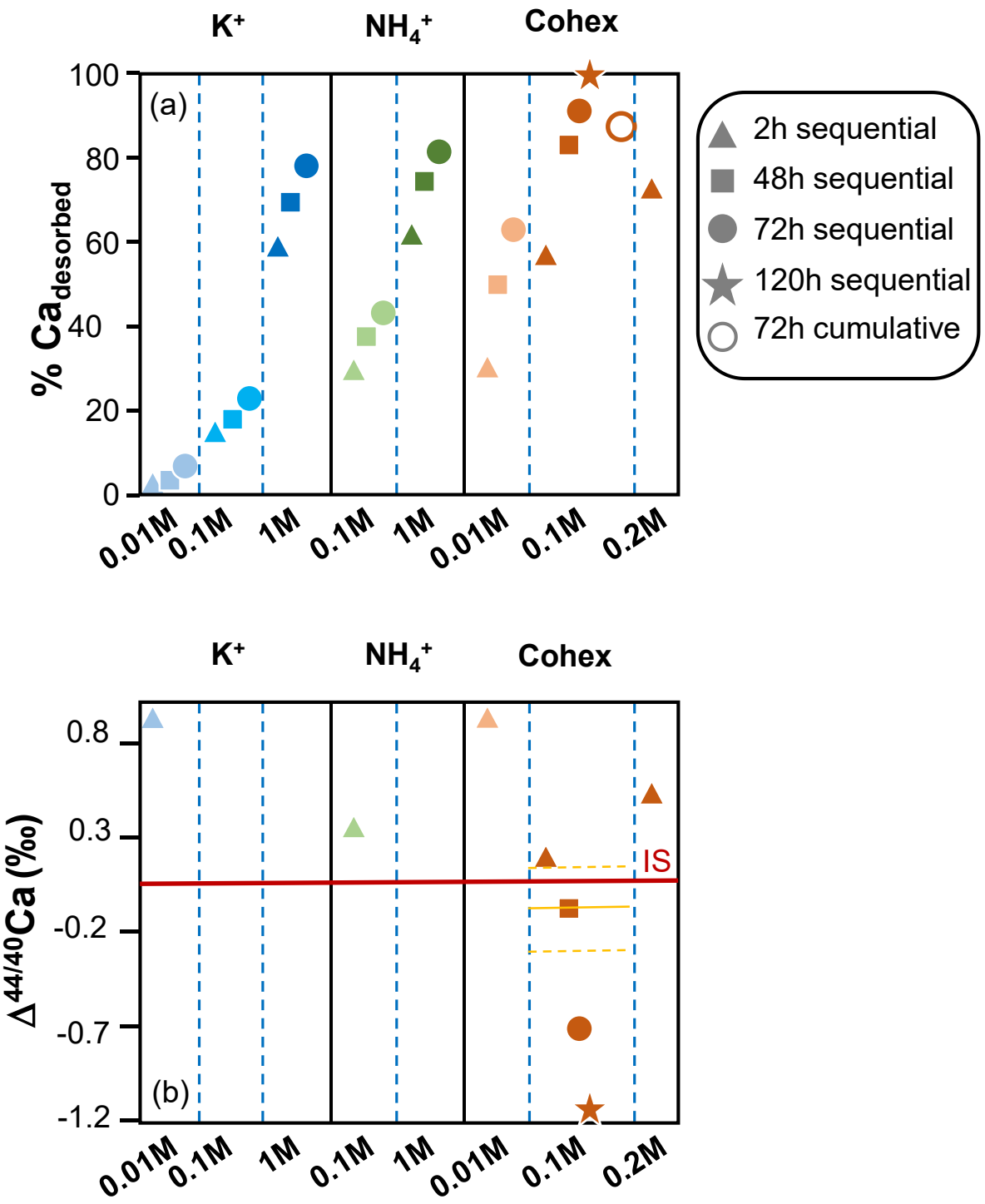

1036

1037

1038

1039 **Fig. 3**

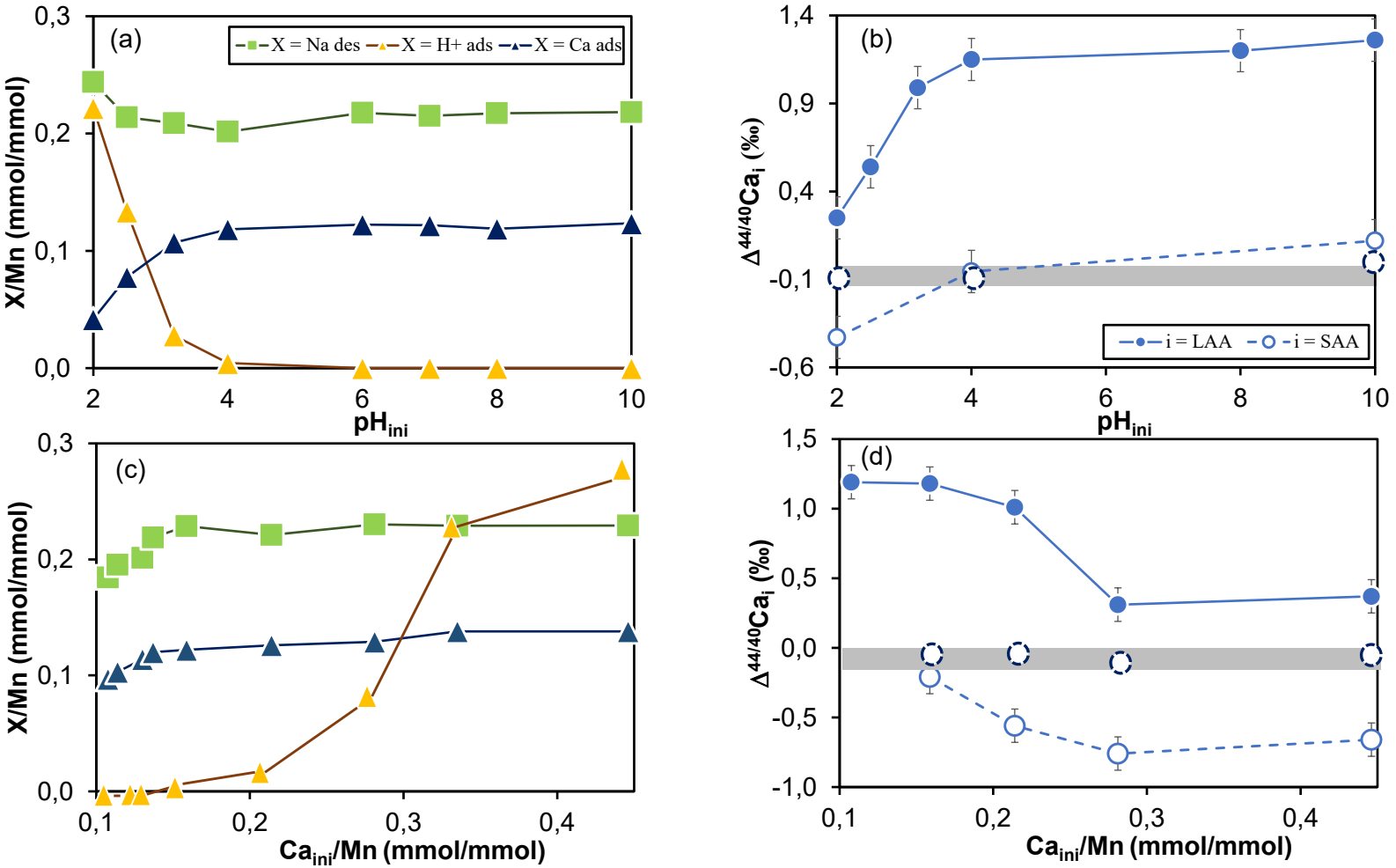

1040

1041

1042 **Fig. 4**

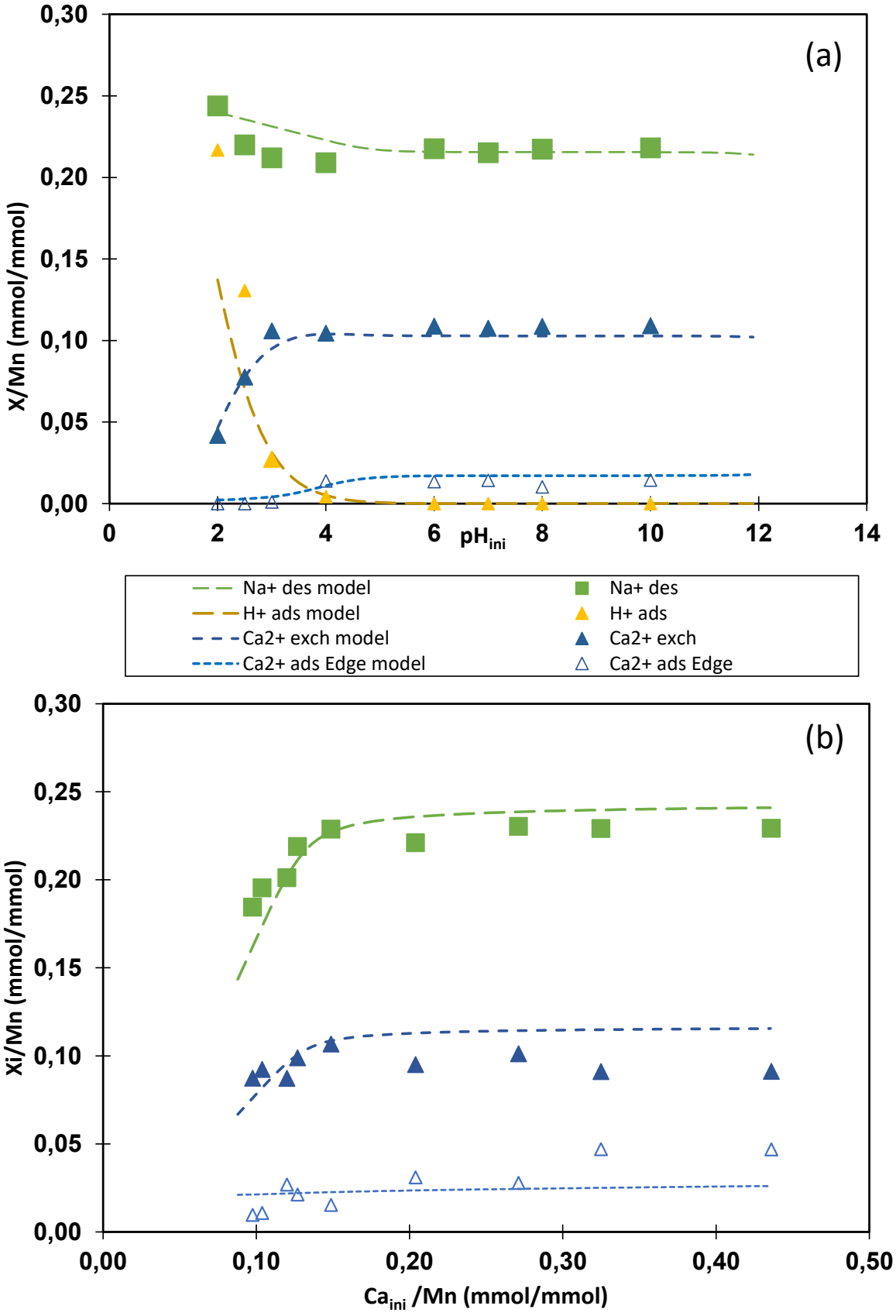

1043

Fig. 5

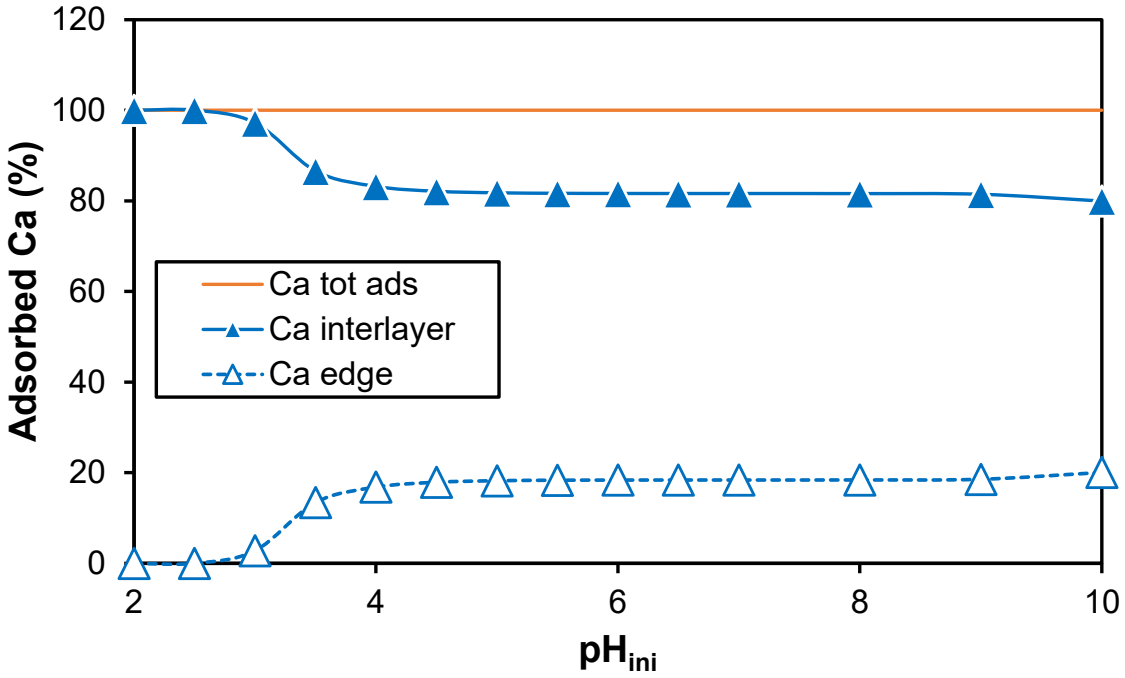
120
100
80
60
40
20
0
Adsorbed Ca (%)
Ca tot ads
Ca interlayer
Ca edge
2
4
6
8
10
pH ini

Fig. 6

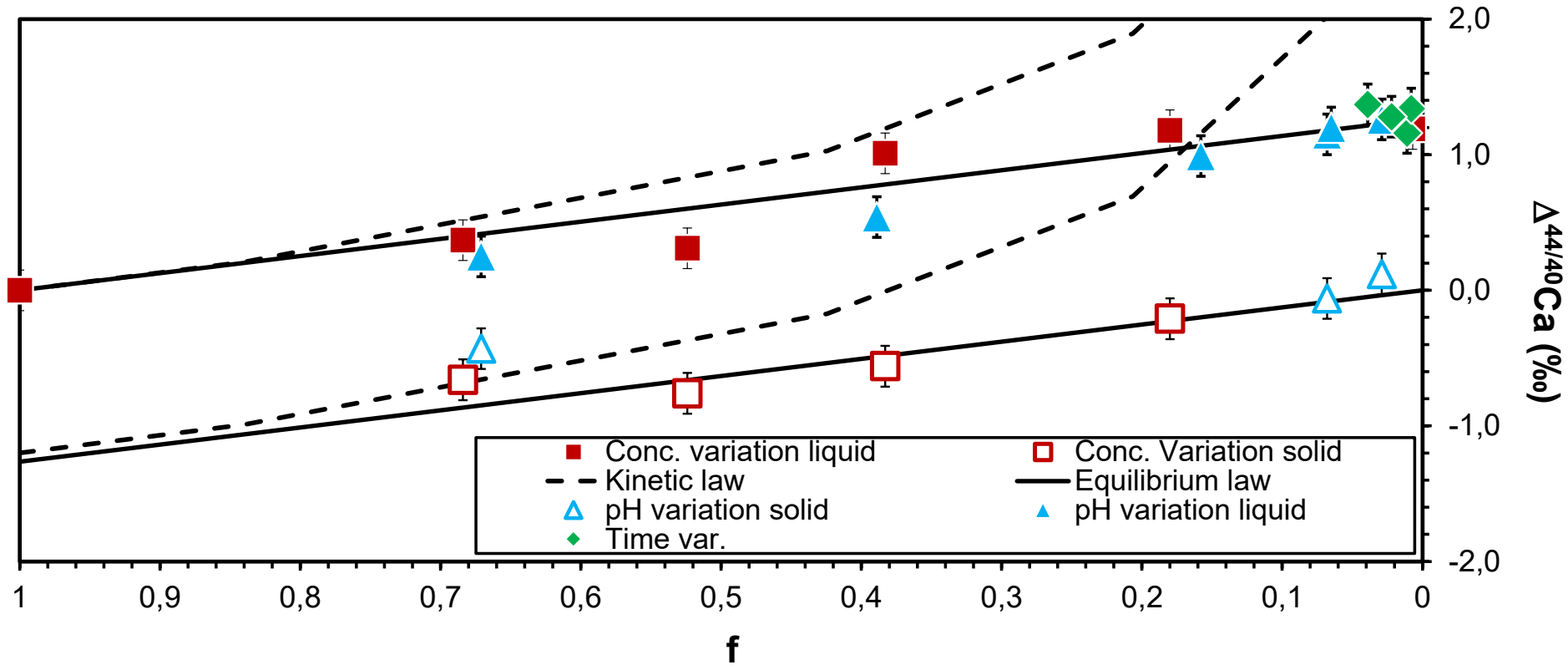
2,0
1,0
0,0
-1,0
-2,0
Δ44/40Ca (‰)
1
0,9
0,8
0,7
0,6
0,5
0,4
0,3
0,2
0,1
0
f
Conc. variation liquid
Conc. Variation solid
Kinetic law
Equilibrium law
pH variation solid
pH variation liquid
Time var.

Table 1

Permanently charged sites (Vacancies)

Cation exchange reaction	Selectivity coefficients	K_{sel}
$2{>}X\text{-}H + Ca^{2+} \leftrightarrow {>}X_2Ca + 2H^+$	$K_{sel\,(2H^+/Ca^{2+})} = \frac{E_{Ca}.\,\{H^+\}^2}{E_H{}^2.\,\{Ca^{2+}\}}$	0.33
$2{>}X\text{-}Na + Ca^{2+} \leftrightarrow {>}X_2Ca + 2Na^+$	$K_{sel\,(2Na^+/Ca^{2+})} = \frac{E_{Ca}.\,\{Na^+\}^2}{E_{Na}{}^2.\,\{Ca^{2+}\}}$	3.33

Sites concentration 2.15 x 10^{-3} eq/g
(calculated from CEC)

Variable charge site (edge sites)

Ca sorption reaction on edge for DLM	Surface complexation constants	Log K_{edge}
$>SOH + H^+ \leftrightarrow >SOH_2^+$	$K_{edge\,(SOH/SOH_2^+)} = \frac{[SOH_2^+]}{[SOH]\,.\{H^+\}}\,.exp\left(\frac{F.\varphi_o}{R.T}\right)$	8*
$>SOH \leftrightarrow >SO^- + H^+$	$K_{edge\,(SOH/SO^-)} = \frac{[SO^-].\{H^+\}}{[SOH]}\,.exp\left(\frac{F.\varphi_o}{R.T}\right)$	- 6.1*
$2>SOH + Ca^{2+} \leftrightarrow >Ca(SOH)_2 + 2H^+$	$K_{edge\,(2SOH/Ca(SOH)_2)} = \frac{[Ca(SOH)_2].\{H^+\}^2}{[SOH]^2.\{Ca^{2+}\}}\,.exp\left(\frac{2F.\varphi_o}{R.T}\right)$	-0.689**

Sites concentration 0.54 x 10^{-3} eq/g
(edge concentration = 0.25 x vacancies concentration according to Marafatto et al. (2018))

Table 2

Table 2

Mineral	Grain size (µm)	CEC (meq/100g)	CEC represented by Na^+ in initial solid (%)	BET (N_2) (m^2/g)	Layer charge (/cell)	Interlayer open	pH	Ca_{ads_max} (mmol/g)	$\Delta^{44/40}Ca$ (‰)	Reference
δ-MnO_2	0.1-1	215	99.2	27.6	0.29	yes	4	1.06	1.15	this study
"	"	"	"	"	"	"	7	1.16	1.19	"
Kaolinite (KGa-2)	0.1-1	3.74	94.5	20.14	0	no	4	4.26	0.00	Brazier et al. (2019)
"	"	"	"	"	"	"	7	9.66	"	"
Montmorillonite (Swy-2)	0.1-1	74.6	90.1	28.6	0.6	yes	4	292.9	0.10	"
"	"	"	"	"	"	"	7	293.7	"	"
Tuftane muscovite	0.1-1	46.7	94.2	62.23	2	no	4	57.95	0.22	"
"	"	"	"	"	"	"	7	63.79	0.27	"
"	50-200	0.42	92.7	0.07	2	no	7	0.209	0.00	"

Table 3

Table 3

Reference	pH_{ini}	pH_{fin}	Interaction time (min)	Ca_{LAA} (mmol)	Ca_{ads} (%)	Ca_{LAA}/Mn (mmol/mmol)	Na_{LAA} (mmol)	Na_{LAA}/Mn (mmol/mmol)	$\Delta^{44/40}Ca_{LAA\_1}$ (‰)	$\Delta^{44/40}Ca_{LAA\_2}$ (‰)	$\Delta^{44/40}Ca_{LAA\_mean}$ (‰)
AdsMnO-0.1 pH7 0m	7	-	5	0.00852	82.0	0.01893	0.078	0.174	1.29	1.33	1.31
AdsMnO-0.1 pH7 5m	"	-	10	0.00482	89.8	0.01072	0.084	0.187	1.00	1.19	1.10
AdsMnO-0.1 pH7 10m	"	-	15	0.00225	95.2	0.00500	0.088	0.196	0.55	0.70	0.63
AdsMnO-0.1 pH7 15m	"	-	20	0.00032	99.3	0.00072	0.092	0.204	-	-	-
AdsMnO-0.1 pH7 30m	"	-	35	0.00052	98.9	0.00116	0.094	0.210	1.08	1.25	1.17
AdsMnO-0.1 pH7 60m	"	-	65	0.00050	98.9	0.00111	0.093	0.207	1.11	1.21	1.16
AdsMnO-0.1 pH7 120m	"	-	125	0.00038	99.2	0.00084	0.091	0.203	1.34	-	1.34
AdsMnO-0.1 pH7 7h	"	-	425	0.00036	99.2	0.00080	0.087	0.193	-	-	-
AdsMnO-0.1 pH7 24h	"	-	1445	0.00104	97.8	0.00231	0.086	0.192	1.28	-	1.28
AdsMnO-0.1 pH7 48h	"	6.8	2885	0.00184	96.1	0.00409	0.090	0.200	1.37	-	1.37

Table 4

Reference	Desorbent	Concentration (mol.L-1)	Interaction time (h:min)	Dead volume (g)	Ca_{LAA} (mmol)	Ca in slurry (mmol)	Ca in desorbent (mmol)	Ca_{ini} (mmol)	Ca_{LAD} (mmol)	Ca_{LAD_corr} (mmol)	Ca_{LAD_corr} (cumulated %)	Ca_{LAD_corr}/Mn (mmol/mmol)	$\Delta^{44/40}Ca_{LAD\_1}$ (‰)	$\Delta^{44/40}Ca_{LAD\_2}$ (‰)	$\Delta^{44/40}Ca_{LAD\_mean}$ (‰)	Slurry and desorbent contribution (‰)	$\Delta^{44/40}Ca_{LAD\_mean\ corr}$ (‰)
aC2pH7	K^+	0.01	2:00	0.31	3.78	0.058	0.03	57.2	0.825	0.73	1.5	0.0016	0.87	-	0.87	0.01	0.86
"	"	"	48:00				"	"	1.34	1.31	4.0	0.0029	-	-	-		
"	"	"	72:00				"	"	1.04	1.00	5.9	0.0022	-	-	-		
C2pH7	"	0.1	2:00	0.22	3.78	0.042	"	"	7.89	7.81	14.6	0.0174	-	-	-		
"	"	"	48:00				"	"	2.70	2.67	19.6	0.0059	-	-	-		
C2pH7F	"	"	72:00				"	"	1.93	1.90	23.2	0.0042	-	-	-		
aC2pH7	"	1	2:00	0.34	3.78	0.065	"	"	29.46	29.36	54.5	0.0653	-	-	-		
"	"	"	48:00				"	"	6.26	6.23	66.1	0.0138	-	-	-		
aC2pH7F	"	"	72:00				"	"	3.64	3.60	72.9	0.0080	-	-	-		
bC2pH7	NH_4^+	0.1	2:00	0.20	3.78	0.039	0.05	"	15.95	15.86	29.5	0.0352	-	-	-		
"	"	"	48:00				"	"	4.64	4.59	38.1	0.0102	-	-	-		
"	"	"	72:00				"	"	2.79	2.74	43.3	0.0061	-	-	-		
cC2pH7	"	1	2:00	0.21	3.78	0.040	"	"	33.29	33.20	61.6	0.0738	0.30	-	0.30	0.01	0.29
"	"	"	48:00				"	"	7.45	7.40	75.4	0.0165	-	-	-		
"	"	"	72:00				"	"	3.55	3.50	82.0	0.0078	-	-	-		
dC2pH7	Cohex	0.01	2:00	0.07	3.78	0.014	0.03	"	16.64	16.59	30.8	0.0369	0.90	-	0.90	0.00	0.90
"	"	"	48:00				"	"	11.26	11.23	51.7	0.0250	-	-	-		
dC2pH7F	"	"	72:00				"	"	6.00	5.96	62.8	0.0133	-	-	-		
eC2pH7	"	0.1	2:00	0.20	3.78	0.039	"	"	30.58	30.50	56.6	0.0678	0.13	-	0.13	0.01	0.12
"	"	"	48:00				"	"	14.17	14.14	82.8	0.0314	-0.12	-	-0.12	0.00	-0.12
"	"	"	72:00				"	"	4.54	4.50	91.2	0.0100	-0.77	-	-0.77	0.00	-0.77
eC2pH7F	"	"	120:00				"	"	4.49	4.45	99.5	0.0099	-1.17	-	-1.17	0.00	-1.17
Cc2pH7D4	"	"	72:00	0.22			"	"	47.0	46.96	87.0	0.1043			-		
DesMnO-0.1 pH7 0min	"	0.02	0:05	0.18	8.11	0.072	"	39.2	26.7	26.62	67.9	0.0592	0.35	0.34	0.35	0.01	0.34
DesMnO-0.1 pH7 5min	"	"	0:10	0.12	4.74	0.028	"	42.6	31.12	31.06	73.0	0.0690	0.18	0.19	0.18	0.01	0.17
DesMnO-0.1 pH7 10min	"	"	0:15	0.08	2.37	0.009	"	44.9	33.47	33.43	74.4	0.0743	0.49	0.51	0.49	0.00	0.49
DesMnO-0.1 pH7 15min	"	"	0:20	0.24	0.57	0.007	"	46.7	32.70	32.66	69.9	0.0726	-	-	-		
DesMnO-0.1 pH7 30min	"	"	0:35	0.12	0.58	0.003	"	46.7	33.31	33.27	71.2	0.0739	-	-	-		
DesMnO-0.1 pH7 60min	"	"	1:05	0.16	0.48	0.004	"	46.8	33.67	33.64	71.8	0.0747	0.60	-	0.60	0.01	0.59
DesMnO-0.1 pH7 120min	"	"	2:05	0.09	0.44	0.002	"	46.9	33.08	33.04	70.5	0.0734	0.55	0.60	0.55	0.00	0.55
DesMnO-0.1 pH7 7h	"	"	7:05	0.11	0.12	0.001	"	47.2	33.46	33.42	70.8	0.0743	-	-	-		
DesMnO-0.1 pH7 24h	"	"	24:05	0.09	0.81	0.004	"	46.5	34.29	34.26	73.7	0.0761	0.42	0.41	0.42	0.00	0.42
DesMnO-0.1 pH7 48h	"	"	48:05	0.09	1.66	0.007	"	45.6	34.11	34.07	74.6	0.0757	0.41	-	0.41	0.00	0.41

1075 # Table 5

Reference	C2pH2	C2pH2.5	C2pH3	C2pH4	C2pH6	C2pH7	C2pH8	C2pH10
pH_{ini}	2.0	2.5	3.2	4.0	6.0	7.0	8.0	10.0
pH_{fin}	2.3	3.8	5.2	5.6	6.1	6.2	6.1	6.7
ΔH^+ (mmol/L)	5.0E+00	3.0E+00	6.2E-01	9.7E-02	2.1E-04	6.9E-04	7.3E-04	2.0E-04
Ca_{ads} (mmol)	0.019	0.035	0.048	0.053	0.055	0.055	0.054	0.056
Ca_{ads} (%)	32.9	61.1	84.2	93.2	96.3	95.9	93.5	97.1
[A]: Ca_{ads}/Mn (mmol/mmol)	0.042	0.078	0.107	0.118	0.122	0.122	0.119	0.123
H^+_{ini} (mmol)	2.0E-01	6.3E-02	1.3E-02	2.0E-03	2.0E-05	2.0E-06	2.0E-07	2.0E-09
H^+_{ini}/Mn (mmol/mmol)	4.4E-01	1.4E-01	2.8E-02	4.4E-03	4.4E-05	4.4E-06	4.4E-07	4.4E-09
H^+_{ads} (mmol)	1.0E-01	6.0E-02	1.2E-02	1.9E-03	4.1E-06	1.4E-05	1.5E-05	4.0E-06
$H+_{ads}$/Mn (mmol/mmol)	2.2E-01	1.3E-01	2.8E-02	4.3E-03	9.1E-06	3.1E-05	3.2E-05	8.9E-06
Na_{des} (mmol)	0.110	0.096	0.094	0.091	0.098	0.097	0.098	0.098
[B] : Na_{des}/Mn (mmol/mmol)	0.244	0.214	0.209	0.202	0.218	0.215	0.217	0.218
[A] – [B] (meq/mmol)	<0	<0	0.005	0.035	0.027	0.029	0.020	0.029
$\Delta^{44/40}Ca_{LAA}$ (‰)	0.25	0.54	0.99	1.15	-	-	1.20	1.26
$\Delta^{44/40}Ca_{SAA\_1}$ (‰)	-0.43	-	-	-0.06	-	-	-	0.12
$\Delta^{44/40}Ca_{SAA\_2}$ (‰)				-0.05				
$\Delta^{44/40}Ca_{SAA\_mean}$ (‰)	-0.43			-0.06				0.12

1076

1077 # Table 6

Reference	C8pH7	C6pH7	C1pH7	C2pH7	C3pH7	C4pH7	C5pH7	ADS300pH7	ADS400pH7
pH_{ini}	7	7	7	7	7	7	7	7	7
pH_{fin}	6.36	6.32	6.31	6.22	5.92	5.55	5.00	4.56	4.48
ΔH^+ (mmol/L)	6.7E-06	7.6E-06	7.8E-06	1.0E-05	2.2E-05	5.4E-05	2.0E-04	5.5E-04	6.6E-04
H^+_{des}/Mn (mmol/mmol)	1.5E-05	1.7E-05	1.7E-05	2.2E-05	4.9E-05	1.2E-04	4.4E-04	1.2E-03	1.5E-03
Ca_{ini} (mmol)	0.044	0.047	0.054	0.057	0.067	0.092	0.122	0.146	0.196
[A] : Ca_{ini}/Mn (mmol/mmol)	0.098	0.104	0.120	0.127	0.149	0.204	0.271	0.325	0.436
Ca_{ads} (mmol)	0.044	0.046	0.051	0.054	0.055	0.057	0.058	0.062	0.062
Ca_{ads} (%)	99.3	99.2	95.0	94.5	82.0	61.7	47.6	42.5	31.6
[B]: Ca_{ads}/Mn (mmol/mmol)	0.097	0.103	0.114	0.120	0.122	0.126	0.129	0.138	0.138
Na_{des} (mmol)	0.083	0.084	0.087	0.092	0.094	0.093	0.092	0.107	0.107
Na_{des}/Mn (mmol/mmol)	0.184	0.195	0.201	0.219	0.229	0.221	0.230	0.229	0.229
[A] – [B] (meq/mmol)	0.010	0.011	0.027	0.021	0.015	0.031	0.028	0.047	0.047
$\Delta^{44/40}Ca_{LAA}$ (‰)	1.19	-	-	-	1.18	1.01	0.31	-	0.37
$\Delta^{44/40}Ca_{SAA}$ (‰)	-	-	-	-	-0.21	-0.56	-0.76	-	-0.66

1078

1079

Supplementary materials for

Calcium isotope fractionation associated with adsorption and desorption on/from δ-MnO_2

Schmitt Anne-Désirée[1], Gangloff Sophie[1], Brazier Jean-Michel[1,2], Nuvoli Nicolas[1], Tertre Emmanuel[3]

[1] Université de Strasbourg, CNRS, ENGEES, ITES UMR 7063, 5, rue Descartes, 67084 Strasbourg Cédex, France

[2] Present address: Institute of Applied Geosciences, Graz University of Technology, Rechbauerstrasse 12, 8010 Graz, Austria

[3] Université de Poitiers/CNRS, UMR 7285 IC2MP (équipe HydrASA), B8 rue Albert Turpain, 86073 Poitiers, France

This file includes:

(1) X-ray data of the studied δ-MnO_2: X-ray diffractogram (S1) and XRD raw data (S2)

(2) Comparison of initial and final pH values for experimental and modelled data (S3)

(3) Calculation of $\Delta^{44/40}$Ca isotope signatures in the interlayer and on the edges

X-ray diffractogram of the studied δ-MnO_2 sample

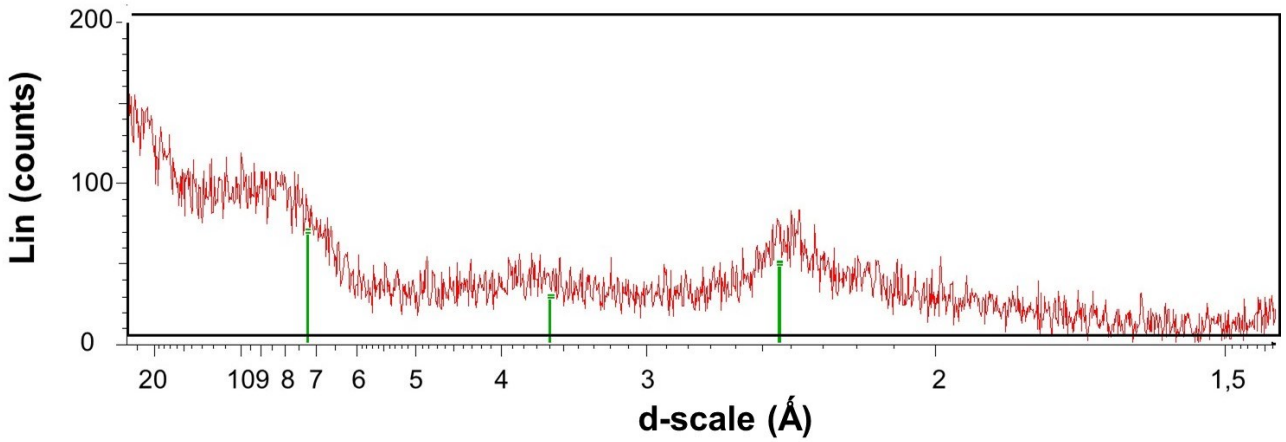

S1: δ-MnO_2 diffractogram after particle size sorting and Na saturation. The attenuation of basal reflections is due to the small size of the coherent domains of δ-MnO_2 and is underlined by the vertical green lines.

S2: XRD raw data

δ-MnO_2 pH7									
X		Y	4.92	17.940	122	6.88	12.833	137
2theta (degrees)	conversion to d (Angström)	Intensity (shots)	4.96	17.795	124	6.92	12.759	112
3.04	29.028	224	5	17.653	129	6.96	12.685	129
3.08	28.651	192	5.04	17.513	114	7	12.613	111
3.12	28.284	222	5.08	17.375	114	7.04	12.541	109
3.16	27.926	205	5.12	17.239	128	7.08	12.471	121
3.2	27.577	186	5.16	17.106	124	7.12	12.401	125
3.24	27.237	172	5.2	16.974	131	7.16	12.331	130
3.28	26.905	175	5.24	16.845	119	7.2	12.263	112
3.32	26.581	162	5.28	16.717	111	7.24	12.195	126
3.36	26.264	211	5.32	16.592	128	7.28	12.128	107
3.4	25.955	172	5.36	16.468	118	7.32	12.062	133
3.44	25.654	157	5.4	16.346	114	7.36	11.997	122
3.48	25.359	164	5.44	16.226	124	7.4	11.932	126
3.52	25.071	163	5.48	16.108	121	7.44	11.868	116
3.56	24.789	150	5.52	15.991	115	7.48	11.805	118
3.6	24.514	157	5.56	15.876	141	7.52	11.742	141
3.64	24.245	149	5.6	15.763	123	7.56	11.680	106
3.68	23.981	147	5.64	15.651	123	7.6	11.618	120
3.72	23.723	141	5.68	15.541	108	7.64	11.558	112
3.76	23.471	168	5.72	15.432	117	7.68	11.498	133
3.8	23.224	164	5.76	15.325	116	7.72	11.438	112
3.84	22.982	144	5.8	15.220	127	7.76	11.379	121
3.88	22.745	146	5.84	15.115	118	7.8	11.321	126
3.92	22.513	132	5.88	15.013	125	7.84	11.263	119
3.96	22.286	157	5.92	14.911	115	7.88	11.206	135
4	22.063	123	5.96	14.811	107	7.92	11.150	127
4.04	21.845	138	6	14.713	114	7.96	11.094	124
4.08	21.631	167	6.04	14.615	109	8	11.038	106
4.12	21.421	130	6.08	14.519	127	8.04	10.984	132
4.16	21.215	133	6.12	14.424	117	8.08	10.929	122
4.2	21.013	121	6.16	14.331	124	8.12	10.876	92
4.24	20.815	132	6.2	14.238	104	8.16	10.822	105
4.28	20.621	131	6.24	14.147	121	8.2	10.770	110
4.32	20.430	120	6.28	14.057	134	8.24	10.717	136
4.36	20.242	132	6.32	13.968	114	8.28	10.666	128
4.4	20.058	110	6.36	13.881	113	8.32	10.615	116
4.44	19.878	146	6.4	13.794	123	8.36	10.564	120
4.48	19.700	142	6.44	13.708	120	8.4	10.514	129
4.52	19.526	115	6.48	13.624	134	8.44	10.464	128
4.56	19.355	137	6.52	13.540	119	8.48	10.415	121
4.6	19.187	141	6.56	13.458	102	8.52	10.366	116
4.64	19.021	129	6.6	13.376	109	8.56	10.317	139
4.68	18.859	131	6.64	13.296	128	8.6	10.270	130
4.72	18.699	109	6.68	13.216	121	8.64	10.222	120
4.76	18.542	104	6.72	13.138	100	8.68	10.175	119
4.8	18.388	121	6.76	13.060	127	8.72	10.129	116
4.84	18.236	143	6.8	12.983	120	8.76	10.082	144
4.88	18.087	139	6.84	12.908	127	8.8	10.037	117

8.84	9.991	122		10.8	8.182	123		12.76	6.929	109
8.88	9.946	126		10.84	8.152	136		12.8	6.908	110
8.92	9.902	138		10.88	8.122	141		12.84	6.886	93
8.96	9.858	129		10.92	8.092	117		12.88	6.865	90
9	9.814	114		10.96	8.063	109		12.92	6.844	93
9.04	9.771	125		11	8.034	124		12.96	6.823	96
9.08	9.728	126		11.04	8.005	117		13	6.802	97
9.12	9.685	128		11.08	7.976	131		13.04	6.781	77
9.16	9.643	104		11.12	7.947	147		13.08	6.761	75
9.2	9.601	129		11.16	7.919	143		13.12	6.740	94
9.24	9.560	116		11.2	7.891	133		13.16	6.720	87
9.28	9.519	112		11.24	7.863	120		13.2	6.699	93
9.32	9.478	121		11.28	7.835	125		13.24	6.679	96
9.36	9.437	136		11.32	7.807	96		13.28	6.659	116
9.4	9.397	124		11.36	7.780	115		13.32	6.639	90
9.44	9.358	116		11.4	7.753	132		13.36	6.619	99
9.48	9.318	123		11.44	7.726	114		13.4	6.600	122
9.52	9.279	108		11.48	7.699	116		13.44	6.580	93
9.56	9.240	125		11.52	7.672	119		13.48	6.561	89
9.6	9.202	144		11.56	7.646	118		13.52	6.541	88
9.64	9.164	136		11.6	7.620	143		13.56	6.522	101
9.68	9.126	114		11.64	7.593	115		13.6	6.503	83
9.72	9.089	120		11.68	7.568	124		13.64	6.484	81
9.76	9.051	133		11.72	7.542	129		13.68	6.465	94
9.8	9.015	128		11.76	7.516	141		13.72	6.447	76
9.84	8.978	111		11.8	7.491	134		13.76	6.428	82
9.88	8.942	143		11.84	7.466	115		13.8	6.409	75
9.92	8.906	121		11.88	7.441	120		13.84	6.391	93
9.96	8.870	107		11.92	7.416	122		13.88	6.373	91
10	8.835	130		11.96	7.391	127		13.92	6.354	93
10.04	8.800	130		12	7.366	111		13.96	6.336	78
10.08	8.765	137		12.04	7.342	132		14	6.318	68
10.12	8.730	124		12.08	7.318	101		14.04	6.300	79
10.16	8.696	134		12.12	7.294	105		14.08	6.283	79
10.2	8.662	144		12.16	7.270	101		14.12	6.265	76
10.24	8.628	131		12.2	7.246	113		14.16	6.247	89
10.28	8.595	138		12.24	7.223	104		14.2	6.230	91
10.32	8.562	148		12.28	7.199	100		14.24	6.212	86
10.36	8.529	156		12.32	7.176	102		14.28	6.195	79
10.4	8.496	102		12.36	7.153	104		14.32	6.178	68
10.44	8.463	124		12.4	7.130	99		14.36	6.161	84
10.48	8.431	118		12.44	7.107	93		14.4	6.144	100
10.52	8.399	134		12.48	7.084	115		14.44	6.127	82
10.56	8.367	131		12.52	7.062	116		14.48	6.110	66
10.6	8.336	111		12.56	7.039	119		14.52	6.093	77
10.64	8.305	136		12.6	7.017	87		14.56	6.076	77
10.68	8.274	123		12.64	6.995	113		14.6	6.060	88
10.72	8.243	104		12.68	6.973	98		14.64	6.043	83
10.76	8.212	127		12.72	6.951	90		14.68	6.027	84

14.72	6.011	74		16.68	5.309	74		18.64	4.755	70
14.76	5.995	70		16.72	5.296	75		18.68	4.745	84
14.8	5.978	77		16.76	5.283	83		18.72	4.734	82
14.84	5.962	80		16.8	5.271	67		18.76	4.724	82
14.88	5.947	60		16.84	5.259	74		18.8	4.714	64
14.92	5.931	68		16.88	5.246	85		18.84	4.705	77
14.96	5.915	75		16.92	5.234	83		18.88	4.695	83
15	5.899	69		16.96	5.222	75		18.92	4.685	71
15.04	5.884	79		17	5.209	65		18.96	4.675	65
15.08	5.868	82		17.04	5.197	72		19	4.665	67
15.12	5.853	75		17.08	5.185	80		19.04	4.656	69
15.16	5.837	79		17.12	5.173	71		19.08	4.646	75
15.2	5.822	76		17.16	5.161	69		19.12	4.636	56
15.24	5.807	82		17.2	5.149	67		19.16	4.627	57
15.28	5.792	58		17.24	5.137	76		19.2	4.617	69
15.32	5.777	85		17.28	5.126	77		19.24	4.608	76
15.36	5.762	78		17.32	5.114	82		19.28	4.598	64
15.4	5.747	74		17.36	5.102	64		19.32	4.589	68
15.44	5.732	86		17.4	5.091	82		19.36	4.579	67
15.48	5.717	79		17.44	5.079	64		19.4	4.570	77
15.52	5.703	80		17.48	5.067	68		19.44	4.561	64
15.56	5.688	64		17.52	5.056	75		19.48	4.551	80
15.6	5.674	79		17.56	5.045	66		19.52	4.542	78
15.64	5.659	85		17.6	5.033	73		19.56	4.533	83
15.68	5.645	75		17.64	5.022	78		19.6	4.524	64
15.72	5.631	76		17.68	5.011	70		19.64	4.515	72
15.76	5.616	58		17.72	4.999	85		19.68	4.506	67
15.8	5.602	73		17.76	4.988	64		19.72	4.497	73
15.84	5.588	63		17.8	4.977	65		19.76	4.488	84
15.88	5.574	73		17.84	4.966	72		19.8	4.479	76
15.92	5.560	65		17.88	4.955	81		19.84	4.470	78
15.96	5.546	68		17.92	4.944	61		19.88	4.461	69
16	5.533	79		17.96	4.933	61		19.92	4.452	79
16.04	5.519	70		18	4.922	71		19.96	4.443	79
16.08	5.505	74		18.04	4.911	79		20	4.434	66
16.12	5.492	56		18.08	4.901	72		20.04	4.425	75
16.16	5.478	82		18.12	4.890	75		20.08	4.417	71
16.2	5.465	75		18.16	4.879	77		20.12	4.408	69
16.24	5.451	77		18.2	4.869	74		20.16	4.399	84
16.28	5.438	62		18.24	4.858	72		20.2	4.391	63
16.32	5.425	85		18.28	4.847	53		20.24	4.382	101
16.36	5.412	57		18.32	4.837	69		20.28	4.374	82
16.4	5.399	73		18.36	4.826	79		20.32	4.365	74
16.44	5.386	83		18.4	4.816	70		20.36	4.357	79
16.48	5.373	63		18.44	4.806	74		20.4	4.348	59
16.52	5.360	68		18.48	4.795	69		20.44	4.340	80
16.56	5.347	93		18.52	4.785	81		20.48	4.331	69
16.6	5.334	80		18.56	4.775	68		20.52	4.323	94
16.64	5.321	70		18.6	4.765	81		20.56	4.315	78

20.6	4.306	64		22.56	3.937	103		24.52	3.626	79
20.64	4.298	82		22.6	3.930	91		24.56	3.620	97
20.68	4.290	83		22.64	3.923	91		24.6	3.615	68
20.72	4.282	57		22.68	3.916	77		24.64	3.609	74
20.76	4.274	70		22.72	3.909	92		24.68	3.603	80
20.8	4.265	78		22.76	3.902	81		24.72	3.597	74
20.84	4.257	79		22.8	3.896	75		24.76	3.592	82
20.88	4.249	83		22.84	3.889	74		24.8	3.586	82
20.92	4.241	84		22.88	3.882	72		24.84	3.580	74
20.96	4.233	61		22.92	3.876	74		24.88	3.574	67
21	4.225	79		22.96	3.869	74		24.92	3.569	75
21.04	4.217	71		23	3.862	75		24.96	3.563	86
21.08	4.209	66		23.04	3.856	86		25	3.558	69
21.12	4.202	77		23.08	3.849	85		25.04	3.552	94
21.16	4.194	78		23.12	3.842	74		25.08	3.546	82
21.2	4.186	68		23.16	3.836	92		25.12	3.541	79
21.24	4.178	85		23.2	3.829	77		25.16	3.535	74
21.28	4.170	71		23.24	3.823	81		25.2	3.530	62
21.32	4.163	92		23.28	3.816	87		25.24	3.524	82
21.36	4.155	79		23.32	3.810	84		25.28	3.519	78
21.4	4.147	86		23.36	3.803	92		25.32	3.513	72
21.44	4.140	75		23.4	3.797	81		25.36	3.508	72
21.48	4.132	75		23.44	3.791	75		25.4	3.502	71
21.52	4.124	63		23.48	3.784	85		25.44	3.497	80
21.56	4.117	68		23.52	3.778	71		25.48	3.492	79
21.6	4.109	66		23.56	3.772	70		25.52	3.486	69
21.64	4.102	80		23.6	3.765	64		25.56	3.481	76
21.68	4.094	83		23.64	3.759	84		25.6	3.476	81
21.72	4.087	81		23.68	3.753	80		25.64	3.470	74
21.76	4.079	87		23.72	3.747	100		25.68	3.465	84
21.8	4.072	80		23.76	3.740	77		25.72	3.460	74
21.84	4.065	79		23.8	3.734	74		25.76	3.454	59
21.88	4.057	72		23.84	3.728	81		25.8	3.449	61
21.92	4.050	75		23.88	3.722	88		25.84	3.444	75
21.96	4.043	84		23.92	3.716	88		25.88	3.439	78
22	4.035	85		23.96	3.710	79		25.92	3.433	78
22.04	4.028	68		24	3.703	92		25.96	3.428	79
22.08	4.021	84		24.04	3.697	78		26	3.423	74
22.12	4.014	66		24.08	3.691	66		26.04	3.418	85
22.16	4.007	82		24.12	3.685	75		26.08	3.413	82
22.2	4.000	73		24.16	3.679	80		26.12	3.408	71
22.24	3.992	65		24.2	3.673	72		26.16	3.402	64
22.28	3.985	74		24.24	3.667	74		26.2	3.397	71
22.32	3.978	81		24.28	3.661	65		26.24	3.392	69
22.36	3.971	75		24.32	3.655	89		26.28	3.387	81
22.4	3.964	79		24.36	3.650	83		26.32	3.382	74
22.44	3.957	81		24.4	3.644	97		26.36	3.377	80
22.48	3.950	76		24.44	3.638	86		26.4	3.372	75
22.52	3.943	76		24.48	3.632	80		26.44	3.367	73

26.48	3.362	88		28.44	3.135	75		30.4	2.937	72
26.52	3.357	67		28.48	3.130	70		30.44	2.933	65
26.56	3.352	67		28.52	3.126	78		30.48	2.929	60
26.6	3.347	71		28.56	3.122	56		30.52	2.926	71
26.64	3.342	68		28.6	3.117	75		30.56	2.922	77
26.68	3.337	80		28.64	3.113	67		30.6	2.918	60
26.72	3.332	79		28.68	3.109	72		30.64	2.914	85
26.76	3.327	61		28.72	3.105	73		30.68	2.911	70
26.8	3.323	79		28.76	3.100	82		30.72	2.907	63
26.84	3.318	54		28.8	3.096	78		30.76	2.903	65
26.88	3.313	75		28.84	3.092	60		30.8	2.900	70
26.92	3.308	87		28.88	3.088	75		30.84	2.896	74
26.96	3.303	71		28.92	3.084	67		30.88	2.892	79
27	3.298	60		28.96	3.079	53		30.92	2.889	78
27.04	3.294	94		29	3.075	56		30.96	2.885	86
27.08	3.289	71		29.04	3.071	61		31	2.881	73
27.12	3.284	71		29.08	3.067	78		31.04	2.878	67
27.16	3.279	66		29.12	3.063	80		31.08	2.874	60
27.2	3.275	80		29.16	3.059	78		31.12	2.870	60
27.24	3.270	79		29.2	3.055	61		31.16	2.867	74
27.28	3.265	61		29.24	3.051	74		31.2	2.863	72
27.32	3.261	68		29.28	3.047	85		31.24	2.860	59
27.36	3.256	85		29.32	3.042	69		31.28	2.856	76
27.4	3.251	72		29.36	3.038	63		31.32	2.853	71
27.44	3.247	76		29.4	3.034	77		31.36	2.849	77
27.48	3.242	80		29.44	3.030	64		31.4	2.846	74
27.52	3.237	78		29.48	3.026	67		31.44	2.842	63
27.56	3.233	68		29.52	3.022	61		31.48	2.838	68
27.6	3.228	68		29.56	3.018	63		31.52	2.835	71
27.64	3.223	74		29.6	3.014	72		31.56	2.831	56
27.68	3.219	84		29.64	3.010	70		31.6	2.828	62
27.72	3.214	81		29.68	3.006	74		31.64	2.824	61
27.76	3.210	70		29.72	3.002	78		31.68	2.821	72
27.8	3.205	60		29.76	2.998	62		31.72	2.818	72
27.84	3.201	65		29.8	2.995	64		31.76	2.814	73
27.88	3.196	66		29.84	2.991	72		31.8	2.811	73
27.92	3.192	66		29.88	2.987	84		31.84	2.807	61
27.96	3.187	81		29.92	2.983	72		31.88	2.804	70
28	3.183	79		29.96	2.979	78		31.92	2.800	64
28.04	3.178	59		30	2.975	72		31.96	2.797	75
28.08	3.174	70		30.04	2.971	74		32	2.794	63
28.12	3.170	77		30.08	2.967	67		32.04	2.790	58
28.16	3.165	82		30.12	2.963	71		32.08	2.787	67
28.2	3.161	57		30.16	2.960	72		32.12	2.783	62
28.24	3.156	65		30.2	2.956	67		32.16	2.780	80
28.28	3.152	72		30.24	2.952	74		32.2	2.777	82
28.32	3.148	85		30.28	2.948	68		32.24	2.773	79
28.36	3.143	70		30.32	2.944	56		32.28	2.770	67
28.4	3.139	75		30.36	2.941	60		32.32	2.767	71

32.36	2.763	64		34.32	2.610	76		36.28	2.473	105
32.4	2.760	73		34.36	2.607	68		36.32	2.471	85
32.44	2.757	83		34.4	2.604	82		36.36	2.468	110
32.48	2.753	70		34.44	2.601	70		36.4	2.465	98
32.52	2.750	74		34.48	2.598	69		36.44	2.463	86
32.56	2.747	82		34.52	2.595	83		36.48	2.460	99
32.6	2.743	87		34.56	2.592	63		36.52	2.457	91
32.64	2.740	99		34.6	2.589	82		36.56	2.455	116
32.68	2.737	77		34.64	2.586	66		36.6	2.452	120
32.72	2.734	58		34.68	2.584	89		36.64	2.450	108
32.76	2.730	55		34.72	2.581	80		36.68	2.447	101
32.8	2.727	77		34.76	2.578	81		36.72	2.445	103
32.84	2.724	82		34.8	2.575	58		36.76	2.442	110
32.88	2.721	70		34.84	2.572	88		36.8	2.439	96
32.92	2.718	73		34.88	2.569	74		36.84	2.437	112
32.96	2.714	75		34.92	2.566	85		36.88	2.434	105
33	2.711	70		34.96	2.563	80		36.92	2.432	122
33.04	2.708	72		35	2.561	70		36.96	2.429	106
33.08	2.705	72		35.04	2.558	76		37	2.427	118
33.12	2.702	69		35.08	2.555	74		37.04	2.424	109
33.16	2.698	65		35.12	2.552	57		37.08	2.422	102
33.2	2.695	87		35.16	2.549	74		37.12	2.419	118
33.24	2.692	54		35.2	2.547	80		37.16	2.417	99
33.28	2.689	68		35.24	2.544	104		37.2	2.414	111
33.32	2.686	79		35.28	2.541	73		37.24	2.412	117
33.36	2.683	68		35.32	2.538	90		37.28	2.409	111
33.4	2.680	78		35.36	2.535	90		37.32	2.407	126
33.44	2.676	82		35.4	2.533	89		37.36	2.404	104
33.48	2.673	85		35.44	2.530	90		37.4	2.402	100
33.52	2.670	82		35.48	2.527	81		37.44	2.399	90
33.56	2.667	67		35.52	2.524	87		37.48	2.397	112
33.6	2.664	86		35.56	2.522	81		37.52	2.394	120
33.64	2.661	78		35.6	2.519	97		37.56	2.392	102
33.68	2.658	73		35.64	2.516	82		37.6	2.389	104
33.72	2.655	74		35.68	2.513	81		37.64	2.387	120
33.76	2.652	82		35.72	2.511	76		37.68	2.384	98
33.8	2.649	71		35.76	2.508	97		37.72	2.382	108
33.84	2.646	88		35.8	2.505	111		37.76	2.380	103
33.88	2.643	86		35.84	2.503	99		37.8	2.377	111
33.92	2.640	60		35.88	2.500	104		37.84	2.375	124
33.96	2.637	78		35.92	2.497	92		37.88	2.372	109
34	2.634	81		35.96	2.494	85		37.92	2.370	112
34.04	2.631	83		36	2.492	75		37.96	2.367	110
34.08	2.628	68		36.04	2.489	86		38	2.365	111
34.12	2.625	80		36.08	2.486	98		38.04	2.363	108
34.16	2.622	77		36.12	2.484	93		38.08	2.360	101
34.2	2.619	68		36.16	2.481	72		38.12	2.358	124
34.24	2.616	76		36.2	2.478	116		38.16	2.356	99
34.28	2.613	81		36.24	2.476	84		38.2	2.353	105

38.24	2.351	92		40.2	2.241	81		42.16	2.141	87
38.28	2.348	99		40.24	2.238	73		42.2	2.139	63
38.32	2.346	98		40.28	2.236	78		42.24	2.137	76
38.36	2.344	90		40.32	2.234	97		42.28	2.135	75
38.4	2.341	91		40.36	2.232	98		42.32	2.133	65
38.44	2.339	92		40.4	2.230	72		42.36	2.131	83
38.48	2.337	101		40.44	2.228	90		42.4	2.129	91
38.52	2.334	104		40.48	2.226	72		42.44	2.127	76
38.56	2.332	87		40.52	2.224	92		42.48	2.125	77
38.6	2.330	128		40.56	2.222	91		42.52	2.124	85
38.64	2.327	98		40.6	2.219	87		42.56	2.122	80
38.68	2.325	100		40.64	2.217	64		42.6	2.120	85
38.72	2.323	89		40.68	2.215	89		42.64	2.118	65
38.76	2.320	112		40.72	2.213	65		42.68	2.116	69
38.8	2.318	95		40.76	2.211	87		42.72	2.114	86
38.84	2.316	97		40.8	2.209	85		42.76	2.112	69
38.88	2.314	83		40.84	2.207	81		42.8	2.110	81
38.92	2.311	116		40.88	2.205	72		42.84	2.108	70
38.96	2.309	91		40.92	2.203	97		42.88	2.107	80
39	2.307	97		40.96	2.201	91		42.92	2.105	79
39.04	2.304	99		41	2.199	97		42.96	2.103	78
39.08	2.302	103		41.04	2.197	90		43	2.101	76
39.12	2.300	107		41.08	2.195	88		43.04	2.099	69
39.16	2.298	97		41.12	2.193	75		43.08	2.097	89
39.2	2.295	79		41.16	2.191	88		43.12	2.095	89
39.24	2.293	81		41.2	2.188	83		43.16	2.094	78
39.28	2.291	81		41.24	2.186	69		43.2	2.092	62
39.32	2.289	93		41.28	2.184	76		43.24	2.090	59
39.36	2.286	94		41.32	2.182	94		43.28	2.088	73
39.4	2.284	95		41.36	2.180	83		43.32	2.086	78
39.44	2.282	97		41.4	2.178	88		43.36	2.084	70
39.48	2.280	96		41.44	2.176	69		43.4	2.083	79
39.52	2.278	78		41.48	2.174	85		43.44	2.081	54
39.56	2.275	87		41.52	2.172	83		43.48	2.079	80
39.6	2.273	84		41.56	2.170	72		43.52	2.077	65
39.64	2.271	98		41.6	2.168	82		43.56	2.075	80
39.68	2.269	90		41.64	2.166	82		43.6	2.073	71
39.72	2.267	100		41.68	2.164	85		43.64	2.072	68
39.76	2.264	91		41.72	2.162	87		43.68	2.070	89
39.8	2.262	98		41.76	2.160	99		43.72	2.068	69
39.84	2.260	81		41.8	2.158	75		43.76	2.066	67
39.88	2.258	89		41.84	2.156	79		43.8	2.064	83
39.92	2.256	94		41.88	2.155	78		43.84	2.063	69
39.96	2.253	88		41.92	2.153	70		43.88	2.061	76
40	2.251	90		41.96	2.151	81		43.92	2.059	68
40.04	2.249	78		42	2.149	79		43.96	2.057	71
40.08	2.247	94		42.04	2.147	75		44	2.055	72
40.12	2.245	85		42.08	2.145	81		44.04	2.054	65
40.16	2.243	96		42.12	2.143	81		44.08	2.052	78

44.12	2.050	70		46.08	1.967	81		48.04	1.892	51
44.16	2.048	64		46.12	1.966	59		48.08	1.890	67
44.2	2.047	96		46.16	1.964	61		48.12	1.889	74
44.24	2.045	70		46.2	1.963	75		48.16	1.887	62
44.28	2.043	69		46.24	1.961	64		48.2	1.886	60
44.32	2.041	65		46.28	1.959	60		48.24	1.884	70
44.36	2.040	70		46.32	1.958	62		48.28	1.883	70
44.4	2.038	62		46.36	1.956	67		48.32	1.881	69
44.44	2.036	88		46.4	1.955	84		48.36	1.880	61
44.48	2.034	71		46.44	1.953	59		48.4	1.878	69
44.52	2.033	67		46.48	1.951	64		48.44	1.877	65
44.56	2.031	60		46.52	1.950	63		48.48	1.875	64
44.6	2.029	89		46.56	1.948	81		48.52	1.874	66
44.64	2.027	76		46.6	1.947	72		48.56	1.873	74
44.68	2.026	71		46.64	1.945	73		48.6	1.871	67
44.72	2.024	71		46.68	1.944	64		48.64	1.870	58
44.76	2.022	70		46.72	1.942	72		48.68	1.868	60
44.8	2.021	65		46.76	1.940	68		48.72	1.867	66
44.84	2.019	67		46.8	1.939	63		48.76	1.865	64
44.88	2.017	72		46.84	1.937	81		48.8	1.864	57
44.92	2.016	85		46.88	1.936	67		48.84	1.863	57
44.96	2.014	75		46.92	1.934	84		48.88	1.861	65
45	2.012	80		46.96	1.933	73		48.92	1.860	72
45.04	2.010	59		47	1.931	51		48.96	1.858	72
45.08	2.009	50		47.04	1.929	66		49	1.857	69
45.12	2.007	63		47.08	1.928	68		49.04	1.855	68
45.16	2.005	63		47.12	1.926	76		49.08	1.854	60
45.2	2.004	57		47.16	1.925	71		49.12	1.853	63
45.24	2.002	72		47.2	1.923	65		49.16	1.851	61
45.28	2.000	54		47.24	1.922	61		49.2	1.850	61
45.32	1.999	70		47.28	1.920	76		49.24	1.848	76
45.36	1.997	66		47.32	1.919	55		49.28	1.847	68
45.4	1.995	71		47.36	1.917	58		49.32	1.845	66
45.44	1.994	60		47.4	1.916	50		49.36	1.844	64
45.48	1.992	80		47.44	1.914	59		49.4	1.843	66
45.52	1.990	84		47.48	1.913	66		49.44	1.841	55
45.56	1.989	88		47.52	1.911	60		49.48	1.840	59
45.6	1.987	65		47.56	1.910	71		49.52	1.839	43
45.64	1.985	53		47.6	1.908	56		49.56	1.837	62
45.68	1.984	76		47.64	1.907	64		49.6	1.836	60
45.72	1.982	67		47.68	1.905	72		49.64	1.834	70
45.76	1.980	74		47.72	1.904	70		49.68	1.833	78
45.8	1.979	71		47.76	1.902	54		49.72	1.832	68
45.84	1.977	68		47.8	1.901	63		49.76	1.830	63
45.88	1.976	57		47.84	1.899	73		49.8	1.829	68
45.92	1.974	74		47.88	1.898	63		49.84	1.827	50
45.96	1.972	76		47.92	1.896	61		49.88	1.826	60
46	1.971	51		47.96	1.895	61		49.92	1.825	53
46.04	1.969	64		48	1.893	58		49.96	1.823	54

50	1.822	66		51.96	1.758	49		53.88	1.700	61
50.04	1.821	67		52	1.757	63		53.92	1.698	54
50.08	1.819	61		52.04	1.755	55		53.96	1.697	52
50.12	1.818	56		52.08	1.754	69		54	1.696	55
50.16	1.817	57		52.12	1.753	53		54.04	1.695	47
50.2	1.815	65		52.16	1.751	37		54.08	1.694	65
50.24	1.814	58		52.2	1.750	40		54.12	1.693	51
50.28	1.812	50		52.24	1.749	68		54.16	1.691	63
50.32	1.811	80		52.28	1.748	45		54.2	1.690	63
50.36	1.810	78		52.32	1.747	61		54.24	1.689	53
50.4	1.808	59		52.36	1.745	62		54.28	1.688	63
50.44	1.807	70		52.4	1.744	58		54.32	1.687	65
50.48	1.806	51		52.44	1.743	65		54.36	1.686	68
50.52	1.804	63		52.48	1.742	70		54.4	1.685	57
50.56	1.803	53		52.52	1.740	65		54.44	1.683	63
50.6	1.802	62		52.56	1.739	54		54.48	1.682	55
50.64	1.800	58		52.6	1.738	60		54.52	1.681	58
50.68	1.799	60		52.64	1.737	53		54.56	1.680	49
50.72	1.798	53		52.68	1.735	62		54.6	1.679	50
50.76	1.796	67		52.72	1.734	52		54.64	1.678	51
50.8	1.795	60		52.76	1.733	51		54.68	1.677	45
50.84	1.794	76		52.8	1.732	61		54.72	1.675	57
50.88	1.793	56		52.84	1.731	59		54.76	1.674	46
50.92	1.791	62		52.88	1.729	64		54.8	1.673	62
50.96	1.790	46		52.92	1.728	59		54.84	1.672	54
51	1.789	63		52.96	1.727	61		54.88	1.671	41
51.04	1.787	47		53	1.726	55		54.92	1.670	48
51.08	1.786	62		53.04	1.724	54		54.96	1.669	61
51.12	1.785	64		53.08	1.723	62		55	1.668	54
51.16	1.783	53		53.12	1.722	59		55.04	1.666	60
51.2	1.782	61		53.16	1.721	66		55.08	1.665	49
51.24	1.781	57		53.2	1.720	59		55.12	1.664	50
51.28	1.779	55		53.24	1.718	65		55.16	1.663	52
51.32	1.778	57		53.28	1.717	71		55.2	1.662	51
51.36	1.777	61		53.32	1.716	56		55.24	1.661	44
51.4	1.776	56		53.36	1.715	46		55.28	1.660	64
51.44	1.774	59		53.4	1.714	57		55.32	1.659	60
51.48	1.773	70		53.44	1.713	69		55.36	1.658	49
51.52	1.772	55		53.48	1.711	78		55.4	1.656	43
51.56	1.770	66		53.52	1.710	61		55.44	1.655	55
51.6	1.769	60		53.56	1.709	63		55.48	1.654	44
51.64	1.768	58		53.6	1.708	61		55.52	1.653	44
51.68	1.767	62		53.64	1.707	67		55.56	1.652	35
51.72	1.765	63		53.68	1.705	48		55.6	1.651	56
51.76	1.764	52		53.72	1.704	58		55.64	1.650	62
51.8	1.763	58		53.76	1.703	55		55.68	1.649	63
51.84	1.762	56		53.8	1.702	57		55.72	1.648	55
51.88	1.760	47		53.84	1.701	60		55.76	1.647	68
51.92	1.759	57		53.88	1.759	61		55.8	1.646	44

55.84	1.644	64		57.8	1.593	53		59.76	1.546	55
55.88	1.643	52		57.84	1.592	73		59.8	1.545	48
55.92	1.642	54		57.88	1.591	53		59.84	1.544	44
55.96	1.641	43		57.92	1.590	54		59.88	1.543	53
56	1.640	60		57.96	1.589	51		59.92	1.542	56
56.04	1.639	59		58	1.588	49		59.96	1.541	51
56.08	1.638	48		58.04	1.587	47		60	1.540	48
56.12	1.637	46		58.08	1.586	46		60.04	1.539	49
56.16	1.636	65		58.12	1.585	39		60.08	1.538	45
56.2	1.635	52		58.16	1.584	59		60.12	1.537	71
56.24	1.634	63		58.2	1.583	48		60.16	1.536	49
56.28	1.633	57		58.24	1.582	61		60.2	1.535	48
56.32	1.632	61		58.28	1.581	63		60.24	1.534	47
56.36	1.631	43		58.32	1.580	44		60.28	1.534	53
56.4	1.629	57		58.36	1.579	41		60.32	1.533	65
56.44	1.628	53		58.4	1.578	54		60.36	1.532	58
56.48	1.627	46		58.44	1.577	59		60.4	1.531	56
56.52	1.626	50		58.48	1.576	52		60.44	1.530	56
56.56	1.625	49		58.52	1.575	57		60.48	1.529	43
56.6	1.624	61		58.56	1.574	37		60.52	1.528	44
56.64	1.623	46		58.6	1.573	39		60.56	1.527	65
56.68	1.622	46		58.64	1.572	59		60.6	1.526	52
56.72	1.621	42		58.68	1.571	52		60.64	1.525	54
56.76	1.620	53		58.72	1.570	60		60.68	1.524	36
56.8	1.619	40		58.76	1.570	39		60.72	1.523	60
56.84	1.618	50		58.8	1.569	39		60.76	1.523	52
56.88	1.617	50		58.84	1.568	56		60.8	1.522	59
56.92	1.616	58		58.88	1.567	53		60.84	1.521	42
56.96	1.615	62		58.92	1.566	44		60.88	1.520	39
57	1.614	61		58.96	1.565	46		60.92	1.519	38
57.04	1.613	50		59	1.564	43		60.96	1.518	37
57.08	1.612	57		59.04	1.563	55		61	1.517	52
57.12	1.611	55		59.08	1.562	56		61.04	1.516	58
57.16	1.610	45		59.12	1.561	50		61.08	1.515	48
57.2	1.609	61		59.16	1.560	47		61.12	1.514	51
57.24	1.608	68		59.2	1.559	45		61.16	1.514	68
57.28	1.606	41		59.24	1.558	52		61.2	1.513	36
57.32	1.605	56		59.28	1.557	57		61.24	1.512	42
57.36	1.604	53		59.32	1.556	47		61.28	1.511	56
57.4	1.603	43		59.36	1.555	49		61.32	1.510	46
57.44	1.602	46		59.4	1.554	59		61.36	1.509	52
57.48	1.601	45		59.44	1.553	46		61.4	1.508	55
57.52	1.600	57		59.48	1.552	51		61.44	1.507	48
57.56	1.599	49		59.52	1.551	48		61.48	1.506	60
57.6	1.598	57		59.56	1.550	52		61.52	1.506	46
57.64	1.597	59		59.6	1.549	39		61.56	1.505	54
57.68	1.596	58		59.64	1.548	54		61.6	1.504	58
57.72	1.595	41		59.68	1.547	50		61.64	1.503	57
57.76	1.594	49		59.72	1.547	54		61.68	1.502	52

61.72	1.501	59		63.68	1.460	59
61.76	1.500	55		63.72	1.459	55
61.8	1.499	48		63.76	1.458	52
61.84	1.499	54		63.8	1.457	45
61.88	1.498	47		63.84	1.456	51
61.92	1.497	50		63.88	1.455	48
61.96	1.496	38		63.92	1.455	50
62	1.495	48		63.96	1.454	42
62.04	1.494	48		64	1.453	64
62.08	1.493	56		64.04	1.452	56
62.12	1.492	45		64.08	1.451	78
62.16	1.492	50		64.12	1.451	52
62.2	1.491	43		64.16	1.450	47
62.24	1.490	50		64.2	1.449	59
62.28	1.489	48		64.24	1.448	63
62.32	1.488	48		64.28	1.447	50
62.36	1.487	52		64.32	1.447	65
62.4	1.486	51		64.36	1.446	58
62.44	1.486	61		64.4	1.445	67
62.48	1.485	62		64.44	1.444	60
62.52	1.484	49		64.48	1.443	65
62.56	1.483	53		64.52	1.443	60
62.6	1.482	43		64.56	1.442	60
62.64	1.481	60		64.6	1.441	51
62.68	1.480	48		64.64	1.440	58
62.72	1.480	65		64.68	1.439	63
62.76	1.479	54		64.72	1.439	63
62.8	1.478	53		64.76	1.438	70
62.84	1.477	50		64.8	1.437	57
62.88	1.476	52		64.84	1.436	68
62.92	1.475	64		64.88	1.435	68
62.96	1.475	37		64.92	1.435	67
63	1.474	39		64.96	1.434	65
63.04	1.473	45		65	1.433	67
63.08	1.472	56				
63.12	1.471	48				
63.16	1.470	55				
63.2	1.470	47				
63.24	1.469	59				
63.28	1.468	49				
63.32	1.467	55				
63.36	1.466	64				
63.4	1.465	46				
63.44	1.465	52				
63.48	1.464	46				
63.52	1.463	47				
63.56	1.462	66				
63.6	1.461	53				
63.64	1.460	53				

1158

Comparison of initial and final pH values for experimental and modelled data

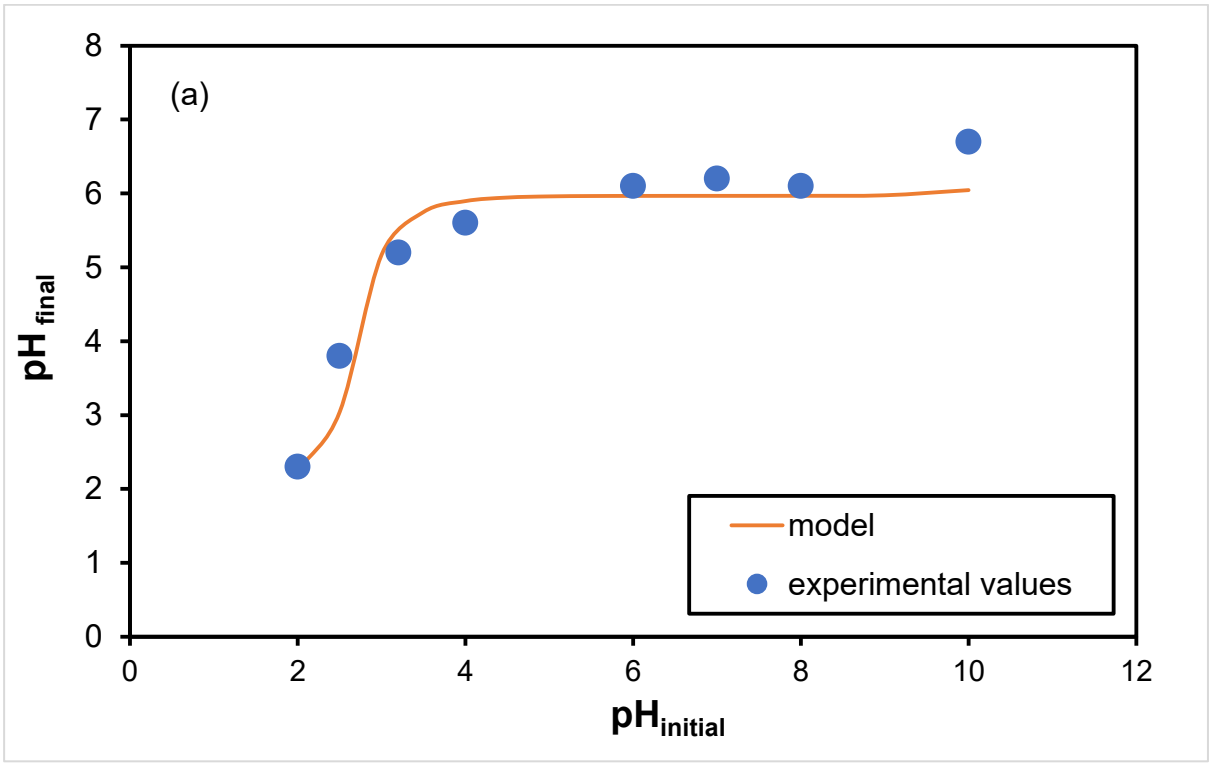

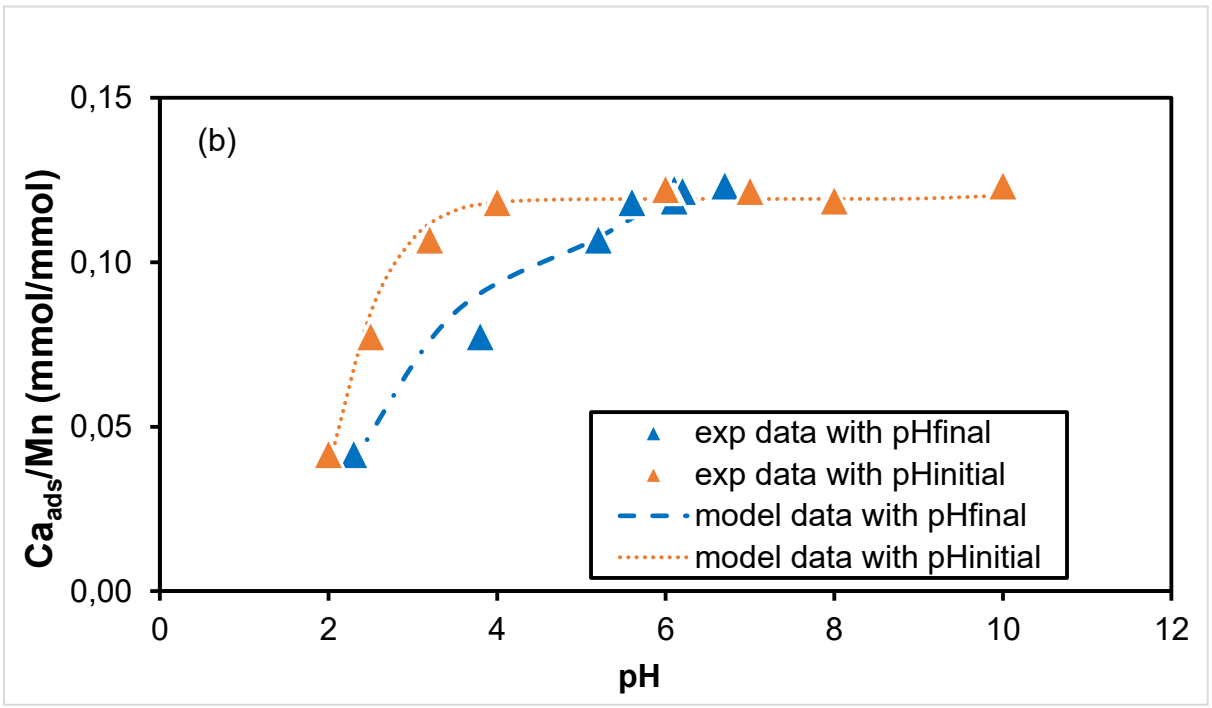

S3: (a) Variation of pH_{final} versus pH_{ini} for model and experimental data and (b) Ca_{ads}/Mn versus pH for model and experimental data (data are plotted for initial and final pH)

1164 Final pH calculated by the model and final experimental ones were plotted in figure S3 (a) as a
1165 function of initial pH (input of the model and fixed experimentally). As seen in the figure, a
1166 good agreement is observed between the two data sets (modeled/experimental). Then,
1167 representation of the Ca-data can be done by using either initial or final pH (figure (b); by using
1168 obviously the same convention for both calculated and measured datasets).

1169

Calculation of $\Delta^{44/40}Ca$ isotope signature in the interlayer and on the edges

$\Delta^{44/40}Ca_{total}$ of the δ-MnO_2 solid at stationary state corresponds to a mixture between the Ca in the interlayer and the Ca bound to the edges:

$$\Delta^{44/40}Ca_{total} = \%_{interlayer} \times \Delta^{44/40}Ca_{interlayer} + \%_{edge} \times \Delta^{44/40}Ca_{edge} \text{ (eq. A.1)}$$

With $\%_{interlayer}$ and $\%_{edge}$ the respective proportions of Ca in the interlayer and on the edges, and $\Delta^{44/40}Ca_{interlayer}$ and $\Delta^{44/40}Ca_{edge}$ the apparent isotope fractionation of Ca in the interlayer and on the edges, respectively

From Table 5, if we consider that for pH <4 Ca is mainly adsorbed in the interlayer, we have

$$\Delta^{44/40}Ca_{interfoliar} \sim -0.43 \text{ ‰}$$

We can therefore propose that at pH 10, the Ca is distributed between the two sites and still using the Ca proportions obtained from the model (c.f. paragraph 4.5), from equation A.1 we obtain

$$\Delta^{44/40}Ca_{edge} \sim 3.5 \text{ ‰}$$